

University of California, Irvine

~ Anteater Air ~

AIAA Design Build Fly

2024-2025

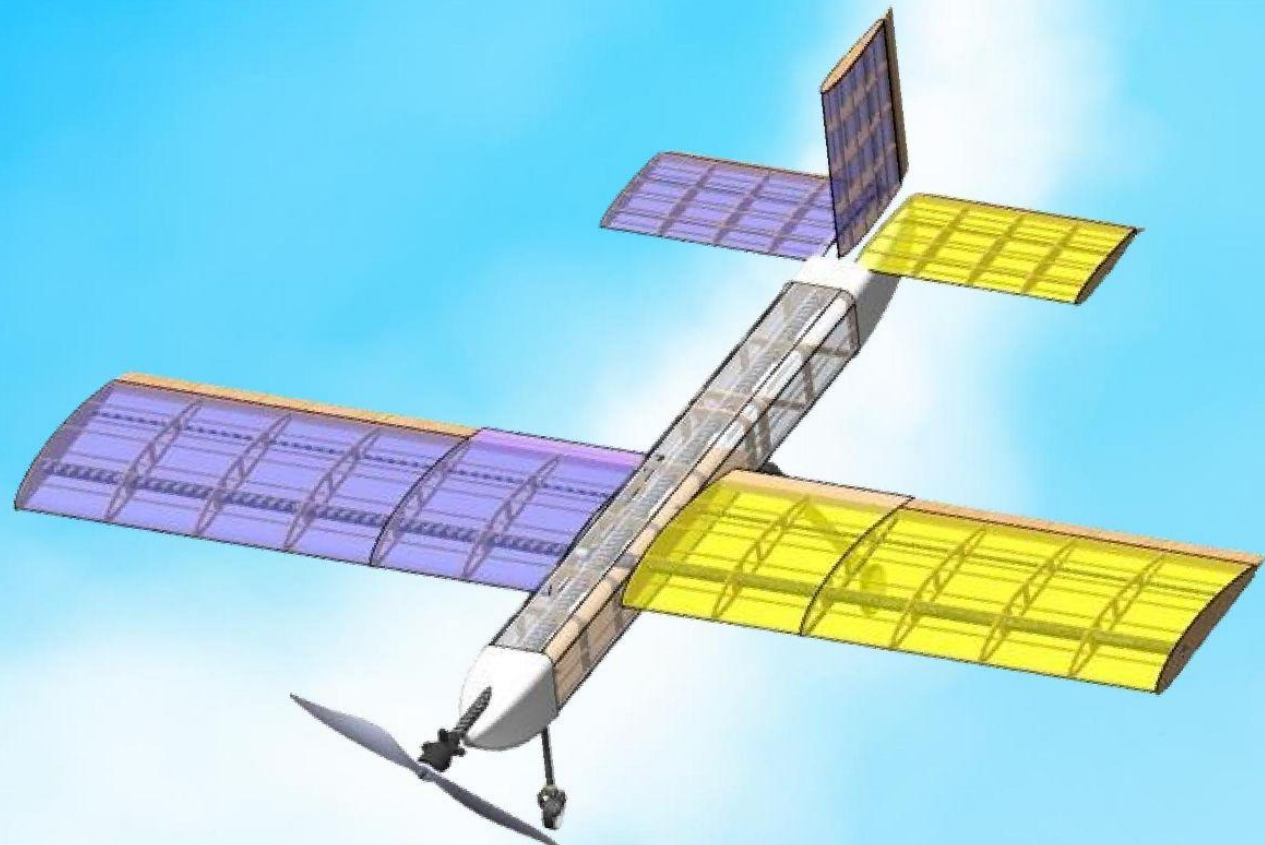


Table of Contents

Table of Contents.....	2
1. Executive Summary.....	4
2. Management Summary.....	4
2.1 Team Organization.....	4
2.2 Milestone Chart.....	5
3. Conceptual Design.....	6
3.1 Mission Requirements.....	6
3.2 Design Goals.....	9
3.3 Scoring Sensitivity.....	10
3.4 Configuration Selection.....	11
3.5 Final Conceptual Design.....	17
4. Preliminary Design.....	17
4.1 Methodology.....	17
4.2 Wing Design.....	18
4.3 Tail Design.....	20
4.4 Propulsion.....	20
4.5 X-1 Test Vehicle.....	21
4.4 Lift and Drag Predictions.....	21
4.5 Stability.....	23
4.6 Predicted Mission Performance.....	25
4.7 Uncertainties.....	25
5. Detail Design.....	26
5.1 Dimension Table.....	26
5.2 Structural Capabilities.....	26
5.3 Subsystem Design.....	28
5.4 Weight and Balance.....	36
5.5 Flight and Mission Performance.....	39
5.6 Drawing Package.....	39
6. Manufacturing Plan.....	40
6.1 Manufacturing Processes.....	40
6.2 Selected Processes.....	41
6.3 Manufacturing Milestones.....	44
7. Testing Plan.....	45
7.1 Testing Schedule.....	45
7.2 Ground Testing.....	45
7.3 Flight Testing.....	49
8. Performance Results.....	51
8.1 Propulsion.....	51
8.2 Structure.....	51
8.3 X-1 Test Vehicle.....	51
9. Bibliography.....	54

Acronyms, Abbreviations, and Symbols

ABS	Acrylonitrile Butadiene Styrene	ESC	Electronic Speed Control
AIAA	American Institute of Aeronautic and Astronautics	FEA	Finite Element Analysis
AGL	Above Ground Level	FoM	Figures of Merit
AR	Aspect Ratio	FoS	Factor of Safety
b	Wing Span	GM	Ground Mission
c	Mean Aerodynamic Chord	It	Tail Moment Arm
CA	Cyanoacrylate	L	Lift Force
CAD	Computer-Aided Design	LiPo	Lithium Polymer
C_D	Coefficient of Drag	M1	Mission 1
C_{Di}	Coefficient of Induced Drag	M2	Mission 2
C_f	Coefficient of Skin Friction	M3	Mission 3
CFD	Computational Fluid Dynamics	NiCad	Nickel-Cadmium
CoG	Center of Gravity	NiMH	Nickel-Metal Hydride
C_L	Coefficient of Lift	ρ	Air Density
C_{lβ}	Sideslip Roll Moment Coefficient	PETG	Polyethylene Terephthalate Glycol
C_{lr}	Yaw Rate Rolling Moment Coefficient	PLA	Polylactic Acid
C_{Mα}	Angle of Attack Pitching Moment Coefficient	q	Dynamic Pressure
C_{Mq}	Pitch Rate Pitching Moment Coefficient	S_h	Planform Area of Horizontal Tail
C_{nβ}	Sideslip Yaw Moment Coefficient	S_{REF}	Planform Area
CNC	Computer Numerical Control	S_{WET}	Wetted Area
C_M	Pitching Moment Coefficient	S_v	Planform Area of Vertical Tail
DBF	Design/Build/Fly	S_w	Planform Area of Wing
e	Oswald Efficiency Factor	SM	Static Margin
		TOFL	Takeoff Field Length
		UCI	University of California, Irvine
		V_H	Horizontal Tail Volume
		V_V	Vertical Tail Volume

1. Executive Summary

This report details the design, manufacturing, and testing of the University of California, Irvine's (UCI) aircraft for the 2024-2025 American Institute of Aeronautics and Astronautics (AIAA) Design/Build/Fly (DBF) competition. The aircraft, named the AnteAtAir, is designed to complete a testing program for the X-1, a supersonic vehicle. Mission 1 (M1) demonstrates the capabilities of an unaltered aircraft without the testing platform installed. Mission 2 (M2) demonstrates a delivery flight with the installation of the X-1 test vehicle and fuel tanks. Mission 3 (M3) demonstrates autonomous control of the vehicle after release from the aircraft mid-flight. Ground Mission (GM) demonstrates the installation of the vehicle and fuel tanks.

In the conceptual design phase, the team analyzed mission scoring, rules, and requirements to configure the aircraft by performing a sensitivity analysis and trade studies. This was followed by the preliminary design phase, where the subsystems of the aircraft were sized according to results from trade studies. The detail design phase encompassed the design of the structure and integration of each subsystem. The completed design features a mid-wing, conventional tail, single-motor, and tricycle gear. The mid-wing balances control and stability while providing the additional clearance for the X-1 test vehicle and bottles. The conventional tail was chosen primarily due to ease of manufacturing and to minimize weight. The single motor was selected to maximize cruise efficiency and minimize weight. The tricycle gear allows for clearance for the X-1 test vehicle and undercarriage access during GM.

In manufacturing, multiple methods and materials were used to meet structural requirements while minimizing weight. The aircraft is primarily constructed using built-up balsa reinforced with carbon fiber tubing capable of holding the full payload and X-1 test vehicle for M2. The X-1 test vehicle is constructed out of foam to reduce weight and minimize manufacturing time.

Design choices were validated through testing. Ground testing was used to evaluate structural integrity and help characterize performance. Flight testing allowed for the collection of data to evaluate flight performance and make necessary adjustments to future designs. Checklists and validations were also implemented to ensure components were functioning within expectations prior to any tests.

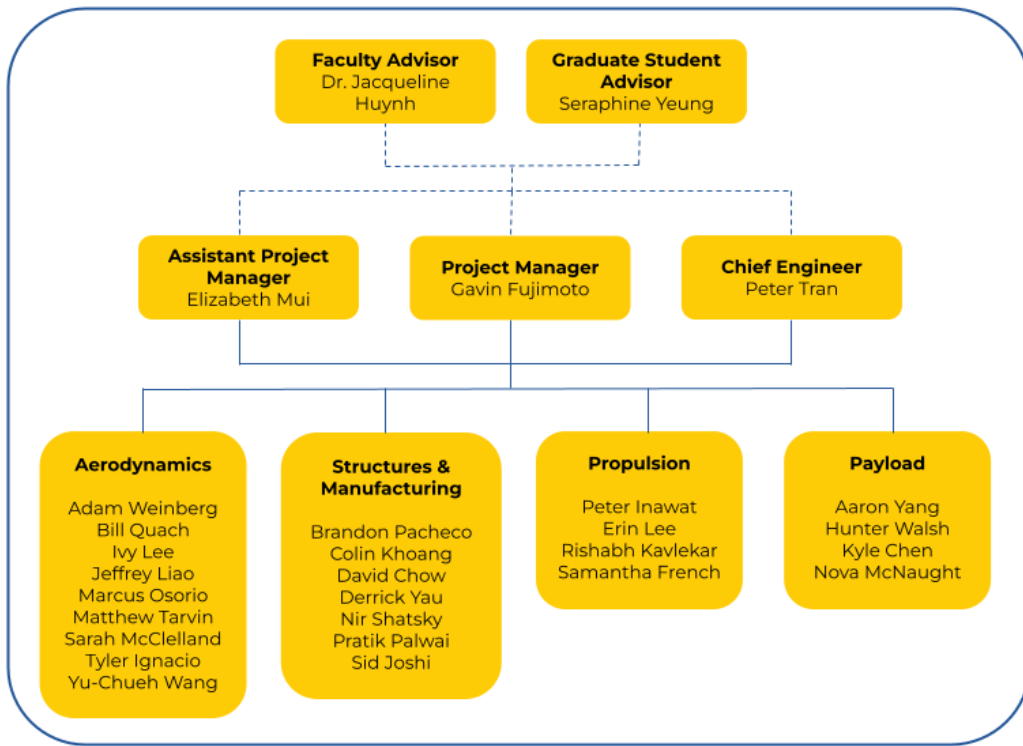
The final design has an empty weight of 6.13 lbs and is capable of finishing M2 in 143.12 seconds while carrying 7 lbs in fuel tank weight, flying 5 laps in M3, completing GM in 70 seconds, and carrying a 0.4. Overall, *AnteAtAir* is predicted to score a total of 5.41 points across all missions.

2. Management Summary

2.1 Team Organization

Design/Build/Fly at UCI is a student-led design project consisting of 26 undergraduate members aided by graduate and faculty advisors. The team consists of 5 seniors and 21 non-seniors. Figure 1 shows the organizational structure of the team. The Project Manager and Assistant Project Manager are responsible for planning, scheduling, cross-team communication, finances, and design considerations. The Chief Engineer is responsible for key technical decisions, including design, analysis, and integration of aircraft components. Collectively, the leads oversee the progress of each of the subteams.

Figure 1: Team Organization



Each subteam is responsible for a distinct subset of tasks, and team members are divided based on their strengths in the needed skills. A breakdown of roles and required skills for each subteam is shown in Table 1.

Table 1: Subteam Roles and Skills

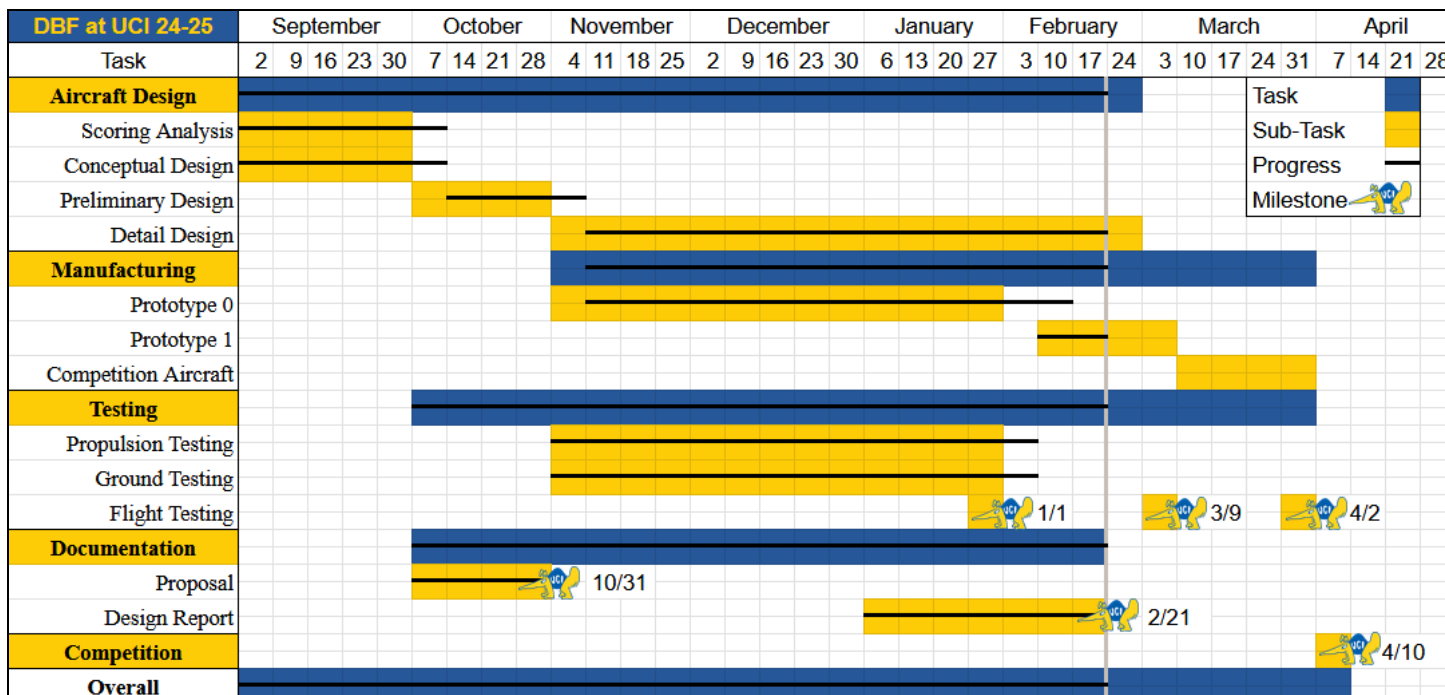
Subteam	Role	Skills
Structures	- Designs and manufactures structural components of the aircraft, including the pylons and X-1 test vehicle attachment - Performs simulations and ground testing to verify structural integrity	- Knowledge of mechanics and materials - Manufacturing - CAD - Structural analysis (FEA)
Aerodynamics	- Performs scoring analysis and trade studies to optimize aircraft design - Sizes and the wing and tails - Conducts CFDs to analyze aircraft performance	- Knowledge of aircraft performance - Aerodynamic analysis (CFD) - Stability analysis (XFLR5) - Scoring analysis (MATLAB)
Propulsion	- Selects electronic package for each mission - Performs testing of battery, motor(s), ESC, and propellers - Collects static thrust data using test rig	- Knowledge of propulsion systems - Performance analysis software (ECalc/MotorCalc) - Wiring and electronics
Payload	- Designs and manufactures the X-1 test vehicle - Conducts research into autonomous control systems	- Manufacturing - CAD - Simulation (FEA/CFD) - Programming flight controller

2.2 Milestone Chart

A Gantt Chart with critical milestones (test flights, proposal and report deadlines, and fly-off) is shown in Figure 2. The Gantt Chart was created at the beginning of the academic year and is used to monitor progress on the development of the aircraft. Components of design, manufacturing, testing, and documentation are included with approximate timelines based on prior experience. The Project Manager maintains the chart and communicates the status of the team's progress. In the event of deviations from the schedule, the Project Manager is responsible for assessing the situation, remedying underlying issues, and reestablishing a realistic workflow.

The Gantt Chart is divided into sections to represent the different phases of development. The aircraft design phase encompasses all aspects of design. Most subtasks within this phase are completed before manufacturing, with the exception of detailed design. The manufacturing phase spans the majority of the aircraft development timeline. During this time, the team focuses on manufacturing prototype and competition aircraft. The testing phase runs concurrently with the manufacturing phase and includes all ground and flight tests performed. Critical milestones are marked, indicating important dates for flight testing, the proposal and design report, and competition.

Figure 2: Gantt Chart



3. Conceptual Design

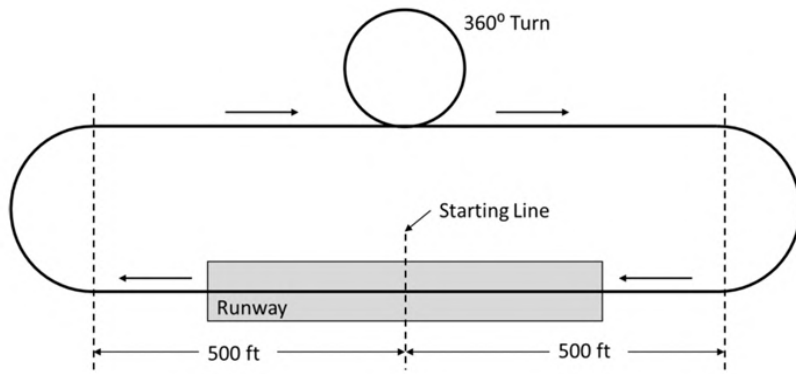
3.1 Mission Requirements

The 2024-25 AIAA DBF Competition challenged students to build an aircraft and autonomous X-1 test vehicle capable of performing an X-1 Supersonic Flight Test Program, including the launch of an X-1 test vehicle. The competition consists of three flight missions and one ground mission: a delivery flight (M1), a captive carry flight (M2), a launch flight (M3), and an X-1 flight test program demonstration (GM).

3.1.1 Staging

Prior to entering the staging box, the external fuel tank pylons will not be installed for M1, but will be installed for M2 and M3. When the aircraft is brought to the staging box prior to each flight, it is in the parked configuration, and the propulsion battery pack(s), fuel tanks, and X-1 test vehicle are removed. Fuel tanks (for M2) and the X-1 test vehicle (for M3) will be weighed and scored by the staging box judge. In five minutes, the team must transition the aircraft to a flight-ready configuration, install the battery, and for M2 and M3, install fuel tanks and the X-1 test vehicle. The team will have another five minutes to complete the flight mission, with the time starting when the throttle is advanced for takeoff. All flight missions are flown along the same path as shown in Figure 3. The aircraft will use ground-rolling takeoff and landing. Laps consist of two 1,000 ft straightaway, two 180° turns, and one 360° turn in the opposite direction of the 180° turns. The completion of a lap is defined by crossing the starting line in the air. A successful landing is required to receive a mission completion score.

Figure 3: Flight Path [1]



3.1.2 Mission 1: Delivery Flight

The objective of M1 is to complete three laps with no payload. One point is awarded if successful (Eq. 1).

$$S_{M1} = 1.0 \text{ for a successful mission}$$

Eq. 1

3.1.3 Mission 2: Captive Carry Flight

The payload for M2 is a minimum of two externally mounted fuel tanks and the X-1 test vehicle. Teams are scored by maximizing the fuel weight while minimizing the time to fly three laps. The team score, indicated by the subscript "UCI" is normalized by the highest weight-to-time ratio, indicated by the subscript "Max" (Eq. 2).

$$S_{M2} = 1 + \frac{(\text{fuel weight/time})_{UCI}}{(\text{fuel weight/time})_{Max}}$$

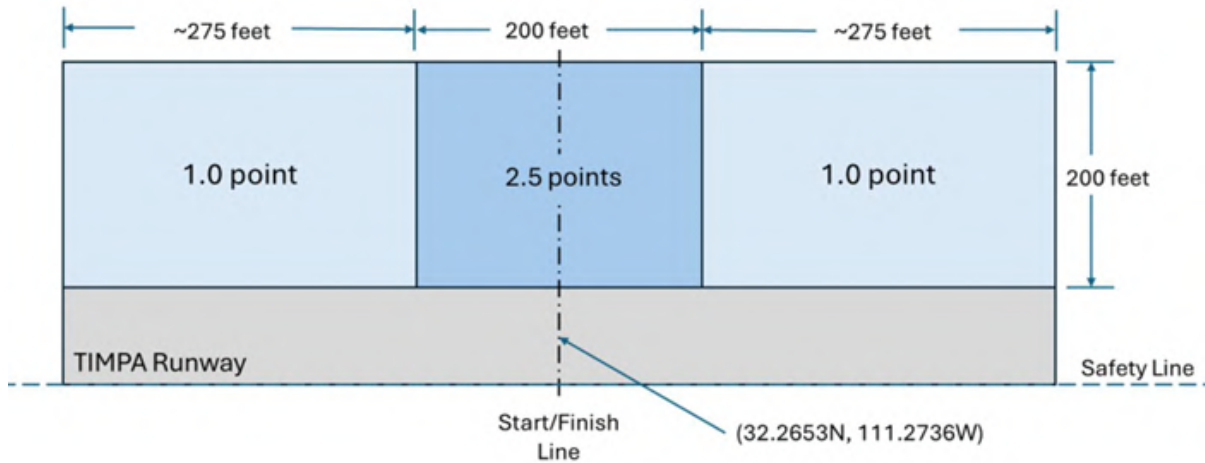
Eq. 2

3.1.4 Mission 3: Launch Flight

The payload for M3 is the X-1 test vehicle and a minimum of two externally mounted fuel tanks, which may be empty. After the aircraft completes the first lap or any subsequent lap, it must reach the required altitude of 200-400 feet AGL, and then the X-1 test vehicle must be launched after crossing the start line and prior to executing the upwind turn. After the X-1 test

vehicle is launched, it must come to rest without crossing the safety line shown in Figure 4, and the aircraft must complete the full lap. The score is a function of the X-1 test vehicle weight, the number of laps flown prior to launch of the X-1 test vehicle, plus any bonus points if the X-1 test vehicle executes a 180° turn after release then descends or orbits to land and rest inside a bonus box (shown in Figure 4) with lights still flashing. Score is normalized by the maximum score achieved by any team (Eq. 3).

Figure 4: Bonus Box Layout [1]



$$S_{M3} = 2 + \frac{(N_{\# \text{ laps flown}} + N_{\text{bonus box score}}/N_{\text{test vehicle weight}})_{UCI}}{(N_{\# \text{ laps flown}} + N_{\text{bonus box score}}/N_{\text{test vehicle weight}})_{Max}}$$

Eq. 3

3.1.5 Ground Mission: X-1 Flight Test Program Demonstration

GM demonstrates how efficiently the aircraft can execute an X-1 Supersonic Flight Test Program by converting from a fleet bomber aircraft to the test program aircraft, installing pylons and fuel tanks, and successfully launching an X-1 test vehicle. The aircraft is brought to the GM staging area with no payloads or components installed and will start and remain on its landing gear during the entire GM. One ground crew member and a pilot participate in GM, and only the ground crew member can touch the aircraft and payloads. The ground crew member is timed for installing all external pylons declared in Tech Inspection. Once verified, the ground crew member is timed again for installing all declared fuel tanks and the X-1 test vehicle and securing and closing all access hatches. Once verified, the pilot confirms all flight controls work properly, then releases the X-1 test vehicle from the aircraft. The lights on the X-1 test vehicle must come on after release. The score for this mission is determined by the time taken, normalized by the lowest time of any team (Eq. 4).

$$S_{GM} = \frac{\text{time}_{Min}}{\text{time}_{UCI}}$$

Eq. 4

3.1.6 Overall Score

The overall score earned by a team is given by the mission scores, Report Score, Proposal Score and Participation Score as shown in Equation 5. Participation scores are awarded as follows: 1 point for attending the Fly-off, 2 points for completing Tech Inspection, and 3 points for attempting a flight mission.

$$\text{Total Score} = (0.15 \times \text{Proposal Score} + 0.85 \times \text{Report Score}) \times (S_{M1} + S_{M2} + S_{M3} + S_{GM}) + \text{Participation Score} \quad \text{Eq. 5}$$

3.1.7 Design Constraints

To transition from the competition rules to physical design parameters, the rules were closely examined to isolate important constraints that strongly influence the design of the aircraft. These constraints are summarized in Table 2.

Table 2: Design Constraints

Category	Constraint
Wings	Wingspan must not exceed 6 feet
	Must be able to pass wingtip load test with maximum declared weight
Propulsion	Must be driven with unmodified off-the-shelf electric motors and propellers
	Propulsion system must use a single NiCad/NiMH or lithium-based battery with the stored energy not exceeding 100 Watt-hours
	Battery must not exceed maximum continuous discharge current of 100 amps
Pylons	Must be removable (and covered by a hatch during M1 if attachment mechanism is internal)
	Must be external to the wing and not obscure or cover the fuel tanks in any way
	Must hold fuel tanks such that there is a discernible gap between the fuel tank and the bottom of the wing
	Adapters must be less than 0.5" tall, 0.5" wide, and 5" long
Fuel Tanks	Must be a commercially available (non-glass) beverage bottle and cannot be modified
	External fuel tanks must all be same size, shape, and brand with minimum capacity of 16 fluid ounces
	At least two external fuel tanks must be installed during M2 and M3
	Must be completely outside of the wing and be attached to the aircraft using pylons
X-1 Test Vehicle	Must be capable of autonomous flight and a commanded release from pilot's transmitter, and have lights flashing after vehicle is released
	Must be carried underneath the aircraft fuselage between left & right external fuel tanks, and have a minimum gap of .25" between its wings and any part of the aircraft fuselage, wings or outer surface
	Must be launched from aircraft at an altitude of 200-400 ft above ground level and land without crossing the safety line
	Must weigh less than 0.55 lbs

3.2 Design Goals

To maximize mission score, the scoring equations were broken down into critical design requirements based on the involved parameters. These are summarized in Table 3 and were used to identify target metrics for the aircraft design. It should be noted that some of the goals conflict; these will require additional analysis to determine the optimal weighting.

Table 3: Design Goals

Mission	Design Goals
M1	Maintain stable flight
M2	Maximize fuel tank weight
	Maximize velocity
M3	Maximize velocity
	Maximize endurance
	Minimize weight of X-1 test vehicle
	Optimize autonomous control of X-1 test vehicle
GM	Minimize time needed to attach pylons, fuel tanks, and X-1 test vehicle

3.3 Scoring Sensitivity

A preliminary analysis of scoring sensitivity was conducted to determine the relative weights of each of the variables in the mission score. Four variables were identified for analysis: fuel tank weight, time to fly 3 laps, number of laps, and X-1 test vehicle weight. For each variable, an initial estimate was made using the average of values from similar aircraft in previous DBF competitions. A summary of the characteristics of these aircraft is included in Table 4. In addition, the values used to normalize the scoring functions were found using values from aircraft with the best performance for that variable. Bonus box points were assumed to be the maximum 2.5 points for both cases since it is independent of the other variables. These values are listed in Table 4. The sensitivity analysis was then performed by plotting the effect of the change in overall score with respect to the change in one of the variables. The results are shown in Figure 5. From our results, minimizing both M2 time and X-1 test vehicle weight were prioritized since they had the highest effect on score.

Figure 5: Scoring Sensitivity Results

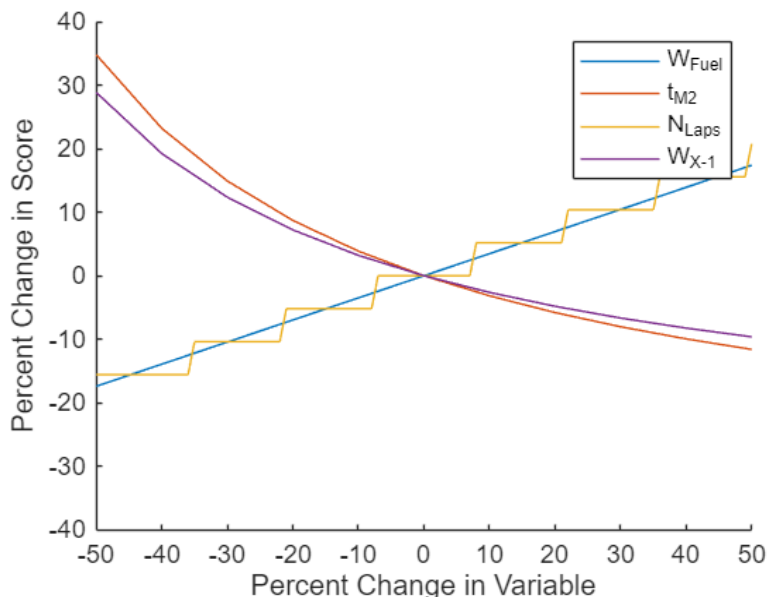


Table 4: Similar Competing Aircraft

	GTech 2020	UCI 2022	UWash 2023	USC 2024
Wing Area [ft ²]	8.5	4.43	6.73	6.58
Cruise Speed [ft/s]	121	60	131	163
Payload Weight [lb]	12.4	3.3	9.33	4.85
Laps Flown (per 5 min.)	5	5	7	8

Table 5: Predicted Team Performance vs Best Performance

	Predicted	Best
Fuel Tank Weight [lbs]	7	12
Time to Fly 3 laps [s]	150	90
Laps flown	6	12
X-1 Test Vehicle Weight [lbs]	0.45	0.30

3.4 Configuration Selection

The optimal aircraft configuration and its components were identified through the down-select process described in Table 6. The chosen Figures of Merit (FoM) are listed below, along with their influence on the scoring.

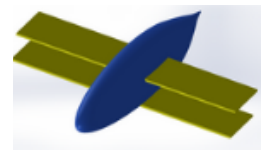
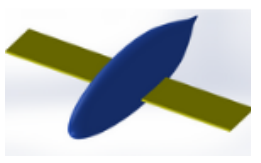
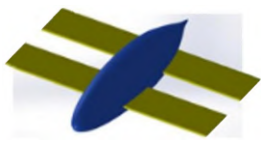
Table 6: Configuration Selection Process

Step #	Description
Step 1	Identify the key aircraft subsystems that need to undergo a configuration selection process
Step 2	Choose relevant Figures of Merit (FoM) for each subsystem and assign a percentage weight to reflect their importance
Step 3	Evaluate each configuration option on a scale of 0 to 5
Step 4	Calculate the total score for each option by finding the sum of the FoM weight multiplied by the assigned 0 to 5 score

3.4.1 Aircraft Configuration

Table 7 shows the three aircraft configurations analyzed: biplane, monoplane, and tandem. The highest-weighted FoM were Lift and Drag, as they directly impact flying mission scores. Although the increased wing area in the biplane and tandem configurations is beneficial for lift, both configurations increase weight, drag, and reduce manufacturability. The conventional monoplane configuration offered the best flight characteristics and manufacturability.

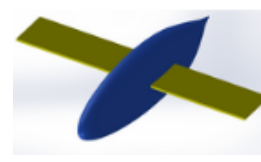
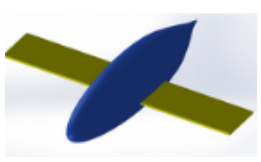
Table 7: Aircraft Configuration Design Matrix

				
Figures of Merit	Weight [%]	Biplane	Monoplane	Tandem
Lift	30	5	3	4
Drag	25	1	4	5
Maneuverability	20	5	3	4
Weight	15	1	3	2
Manufacturability	10	1	5	2
Total Score	100	1.9	3.2	2.9

3.4.2 Wing Placement

Table 8 presents the wing placement options, which include low-wing, mid-wing, and high-wing configurations. The impact on X-1 test vehicle clearance and ground clearance was a key factor in the M2 and M3 scoring. The low-wing configuration was eliminated due to its negative effect on X-1 test vehicle clearance. Both the mid-wing and high-wing configurations did not affect X-1 test vehicle clearance, but the high-wing configuration limited maneuverability. Additionally, manufacturing a high-wing presented more challenges and offered fewer benefits in terms of stability and control. Ultimately, the mid-wing configuration was selected, primarily for its advantages in manufacturability and maneuverability, with added benefits in flight handling and ease of production.

Table 8: Wing Placement Design Matrix

				
Figures of Merit	Weight [%]	High	Mid	Low
X-1 test vehicle Clearance	30	5	4	1
Ground Clearance	25	3	3	1
Parking Options	20	5	5	1
Maneuverability	15	1	3	2
Manufacturability	10	1	3	2
Total Score	100	3.5	3.7	1.25

3.4.3 Wing Planform

Rectangular wings, a fully tapered wing, and a tapered wing with the taper starting a distance away from the root chord were compared in Table 9. In order to evaluate these three fairly, CFD simulations were conducted in SolidWorks to find an optimal taper ratio and taper starting location at our estimated top speed of 115 ft/s while keeping wing area constant. The results are summarized in Figures 6 and 7 and are consistent with literature on the topic [2, p. 110]. Figure 6 shows a rise in L/D at first, peaking around 0.3-0.4 before falling again due to the decrease then increase of the Oswald efficiency factor, e . While having a fully tapered wing does improve lift efficiency, a partially tapered wing seems to provide only minimal improvements over a rectangular wing. Figure 7 plots the distance from the root chord that the taper starts at and shows a general decrease in performance the farther away from the root chord the taper starts at. The difficulty in manufacturing a tapered wing of any kind, alongside the wing stalling at the tips first, made rectangular wings our preferred wing planform.

Figure 6: Lift/Drag Ratio vs Taper Ratio

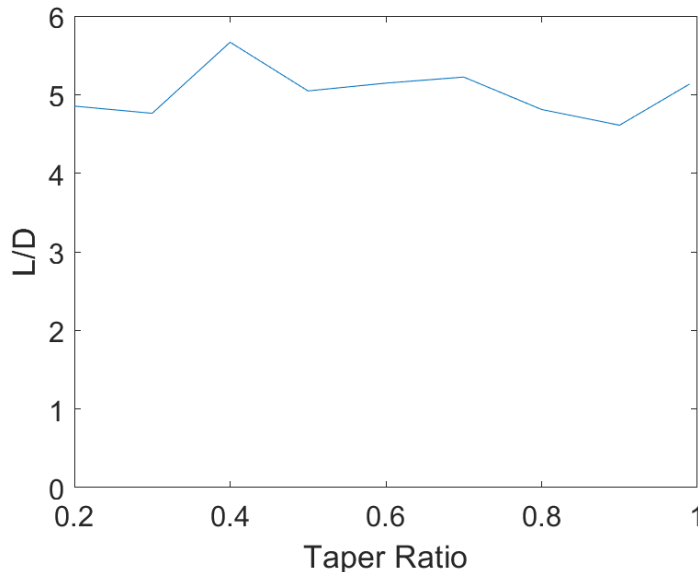


Figure 7: Lift/Drag Ratio vs Taper Start

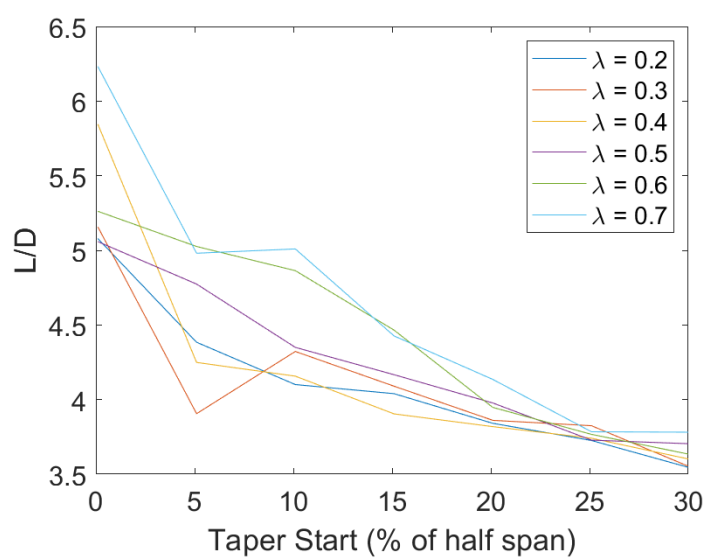


Table 9: Wing Shape Design Matrix

Figures of Merit	Weight [%]	Rectangular	Fully Tapered	Partially Tapered
L/D	40	3	5	3
Manufacturability	40	5	2	3
Stall Characteristics	20	5	4	3
Total Score	100	4.2	3.6	3

3.4.4 Tail Configuration

Table 10 outlines the tail configuration options, including conventional tail, T-tail, and H-tail. The primary factors in the selection process were the tail's aerodynamic effect on the aircraft and the ease of design and fabrication. While both T-tail and H-tail configurations offer aerodynamic benefits by positioning the stabilizers outside the wake of the fuselage, helping reduce drag, they also add structural weight due to reinforcements at the tips of the vertical and horizontal stabilizers. Additionally, integrating a low horizontal stabilizer in a conventional tail is simpler than placing it atop the vertical stabilizer, as required by T-tail and H-tail configurations. The increased weight and complexity of manufacturing T-Tail and H-Tail configurations made them less favorable. As a result, the conventional tail configuration was chosen, as it provided a lighter, more manufacturable solution.

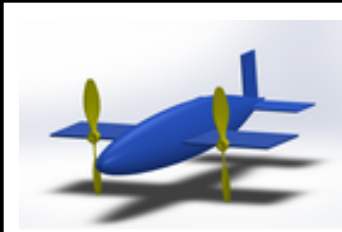
Table 10: Tail Configuration Design Matrix

Figures of Merit	Weight [%]	Conventional	T-Tail	H-Tail
Weight	50	5	3	3
Stability	30	4	5	4
Manufacturability	20	5	3	3
Total Score	100	4.7	3.6	3.3

3.4.5 Propulsion

Table 11 provides a comparison of single-motor and dual-motor configurations, taking into account key factors such as weight, stability, and manufacturability. The single-motor configuration has a higher thrust/weight ratio, eliminates the need for additional components, such as an additional ESC, and requires less structural reinforcement. While the dual-motor configuration may offer increased thrust, redundancy, and enhanced stability in certain situations, it adds complexity to the aircraft's design and operation. The single-motor setup, on the other hand, simplifies both the manufacturing process and overall maintenance. Based on these considerations, the single-motor configuration was selected, offering a better balance between performance, weight, and ease of production compared to the dual-motor option.

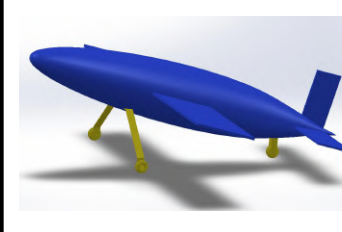
Table 11: Propulsion Design Matrix

			
Figures of Merit	Weight [%]	Single Motor	Dual Motor
Weight	50	5	1
Stability	30	5	5
Manufacturability	20	3	1
Total Score	100	4.6	2.2

3.4.6 Landing Gear

Table 12 compares two landing gear configurations for the aircraft: the tricycle and tail dragger. The tricycle configuration provides higher stability and better support for the X-1 test vehicle because the aircraft remains parallel to the ground and has a higher clearance. In addition, the tricycle configuration allows the main landing gear to be placed closer to the structural hardpoints of the aircraft, reducing manufacturing complexity. The tricycle configuration was selected for these reasons.

Table 12: Landing Gear Design Matrix

			
Figures of Merit	Weight [%]	Tricycle	Tail Dragger
Weight	10	2	3
Drag	20	3	4
Stability	20	5	2
Manufacturability	10	4	3
X-1 Vehicle Support	40	3	2
Total Score	100	3.4	2.6

3.4.7 Fuel Tank

CFD simulations were run in SolidWorks on four different bottle types with the cap facing both forwards and backwards at our expected speed of 75 ft/s; the data is summarized in Figure 9. Images of the velocity flow trajectories can be seen in Figures 8a-d (cap facing forwards on left, cap facing backwards on right). The four bottles were chosen based on being the cheapest and most easily accessible at a Target located nearest to the UCI campus. The Cola bottle, facing backwards, was selected for having the lowest drag characteristics. No bottles were placed inside the fuselage due to the time penalty it would impose for the Ground Mission.

Figure 8: Bottle Simulation Results

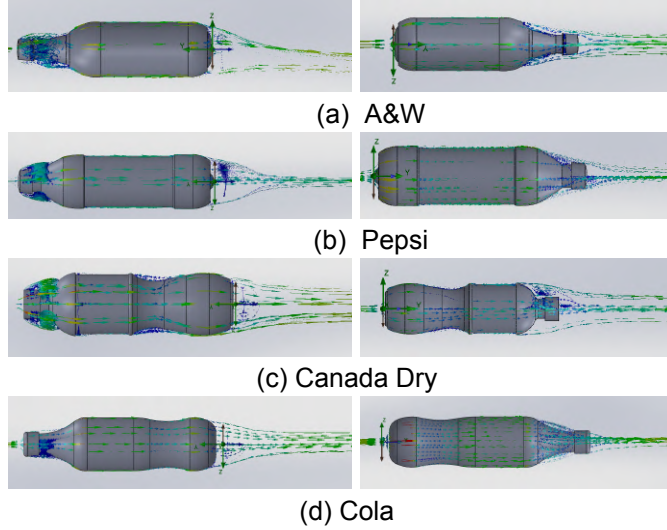
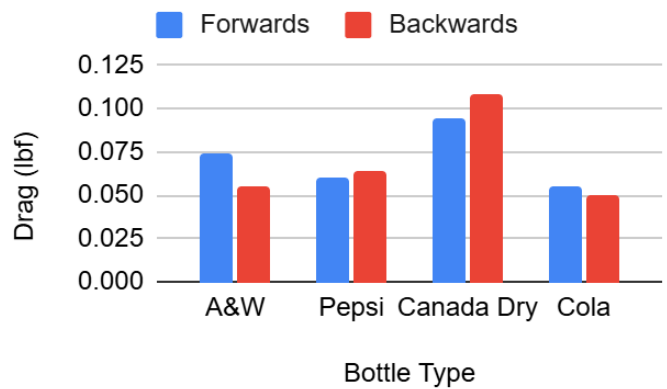


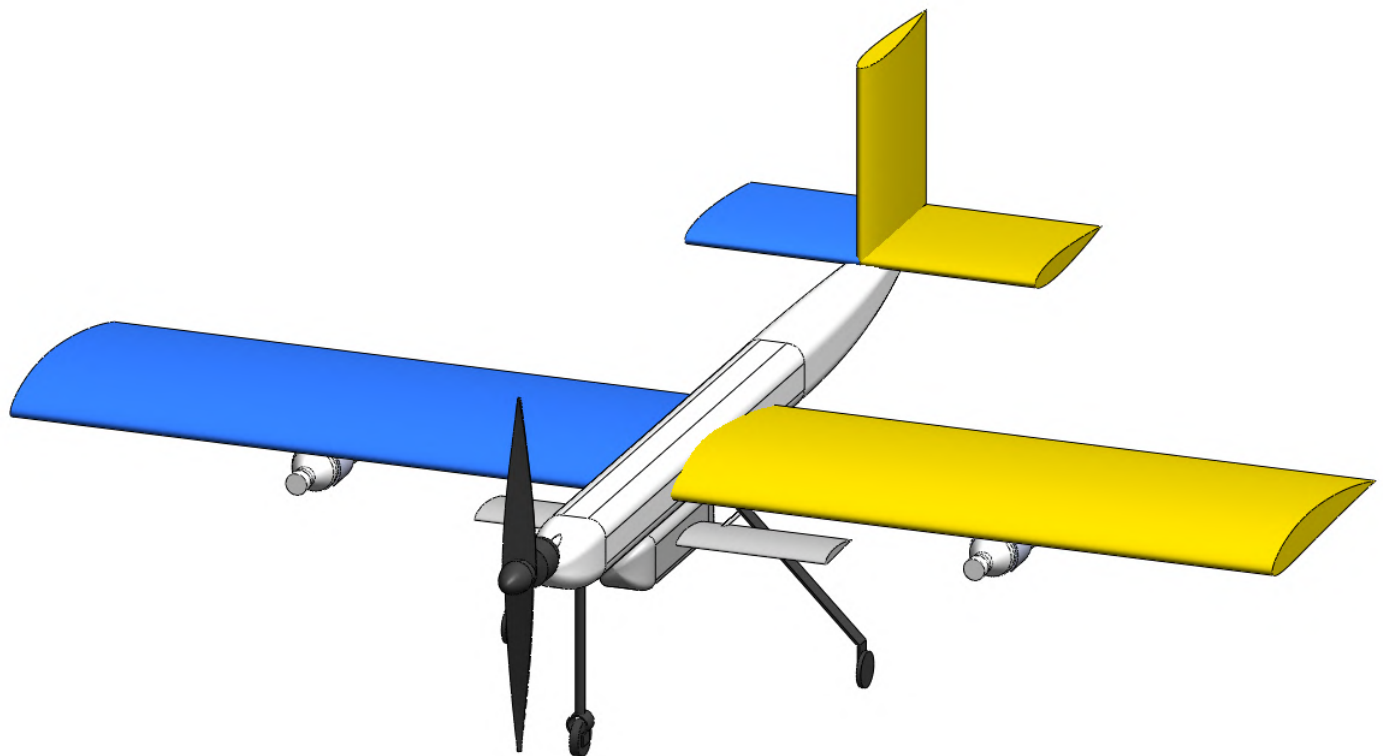
Figure 9: Drag vs Bottle Type



3.5 Final Conceptual Design

The final conceptual design is a monoplane with a rectangular wing placed in the middle of the fuselage, a conventional tail, a single motor, the X-1 test vehicle held underneath the fuselage between the main landing gear, and a single fuel tank attached to the underside of each wing as shown in Figure 10 below.

Figure 10: Final Conceptual Design

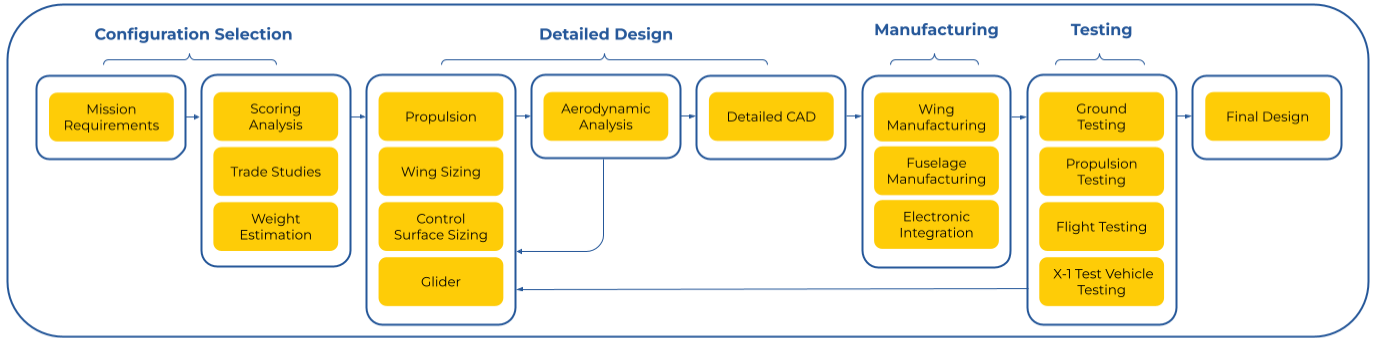


4. Preliminary Design

4.1 Methodology

The design process begins with a configuration being selected based on mission requirements, scoring analysis, and MATLAB-based trade studies. Weight was then estimated before major components of the aircraft—such as the wing, control surfaces, and propulsion—were sized using a combination of hand calculations and simulation software. Static stability, dynamic stability, lift, and drag analysis were then performed using SolidWorks Flow Simulations and XFLR5. Component sizing was adjusted accordingly, and a detailed CAD was created in preparation for manufacturing. Manufacturing utilized primarily laser cutting and 3D printing processes, with testing on prototypes being used shortly after to update the detailed design. This process was repeated until an optimal design was achieved. A flowchart of this design process is shown in Figure 11.

Figure 11: Design Methodology



4.2 Wing Design

The wing was designed to maximize aerodynamic efficiency, structural integrity, and mission performance while adhering to competition constraints. This was accomplished using airfoil analysis, lift and drag calculations, and simulations in MATLAB, XFLR5, and SolidWorks.

4.2.1 Airfoil Selection

Several airfoils were considered: NACA 2412, NACA 4412, NACA 2415, and NACA 4415. The profiles are shown in Figure 12. These airfoils were selected for comparison due to their well-documented aerodynamic properties and favorable geometry for manufacturing. The lift and drag characteristics of the airfoils were compared using data from AirfoilTools at a Reynold's Number of 500,000, approximated from the aircraft's flight conditions. The plots are shown in Figure 13.

Figure 12: Airfoil Profiles

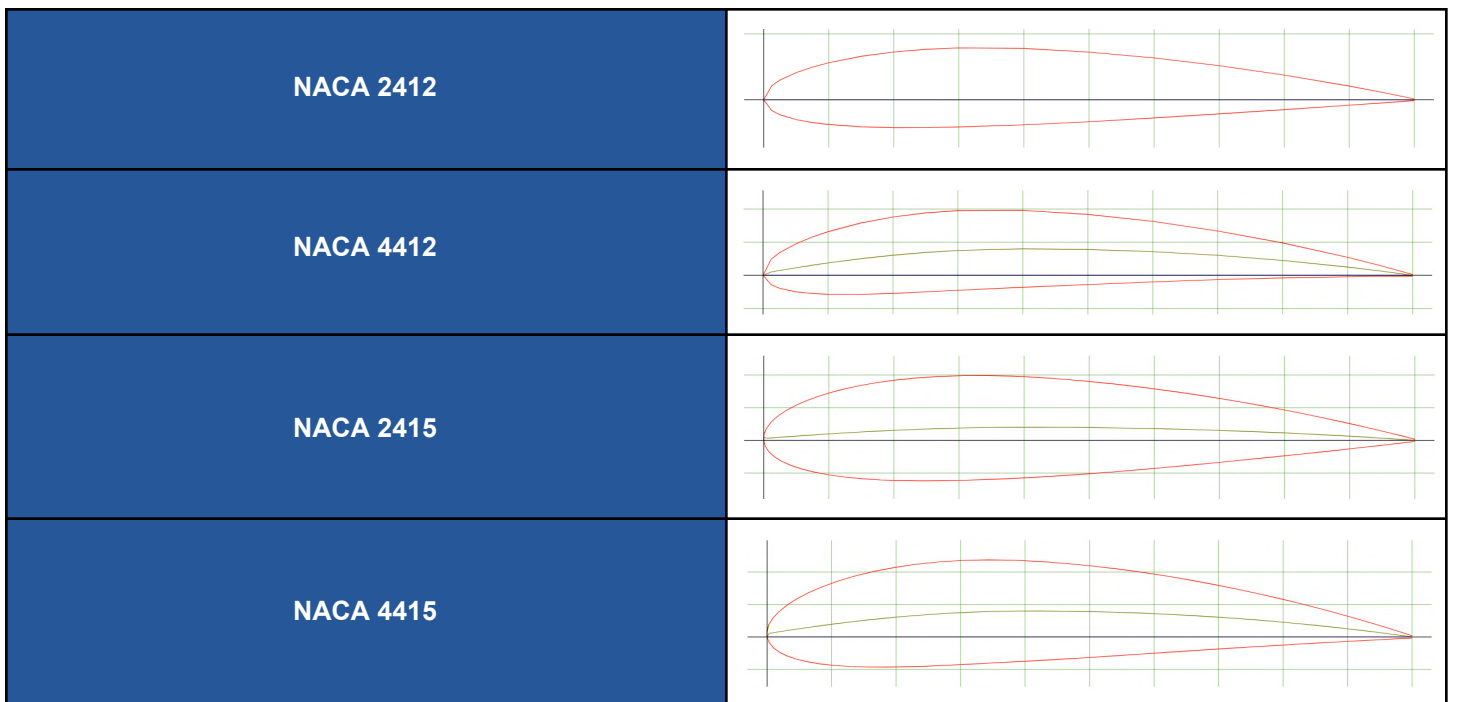
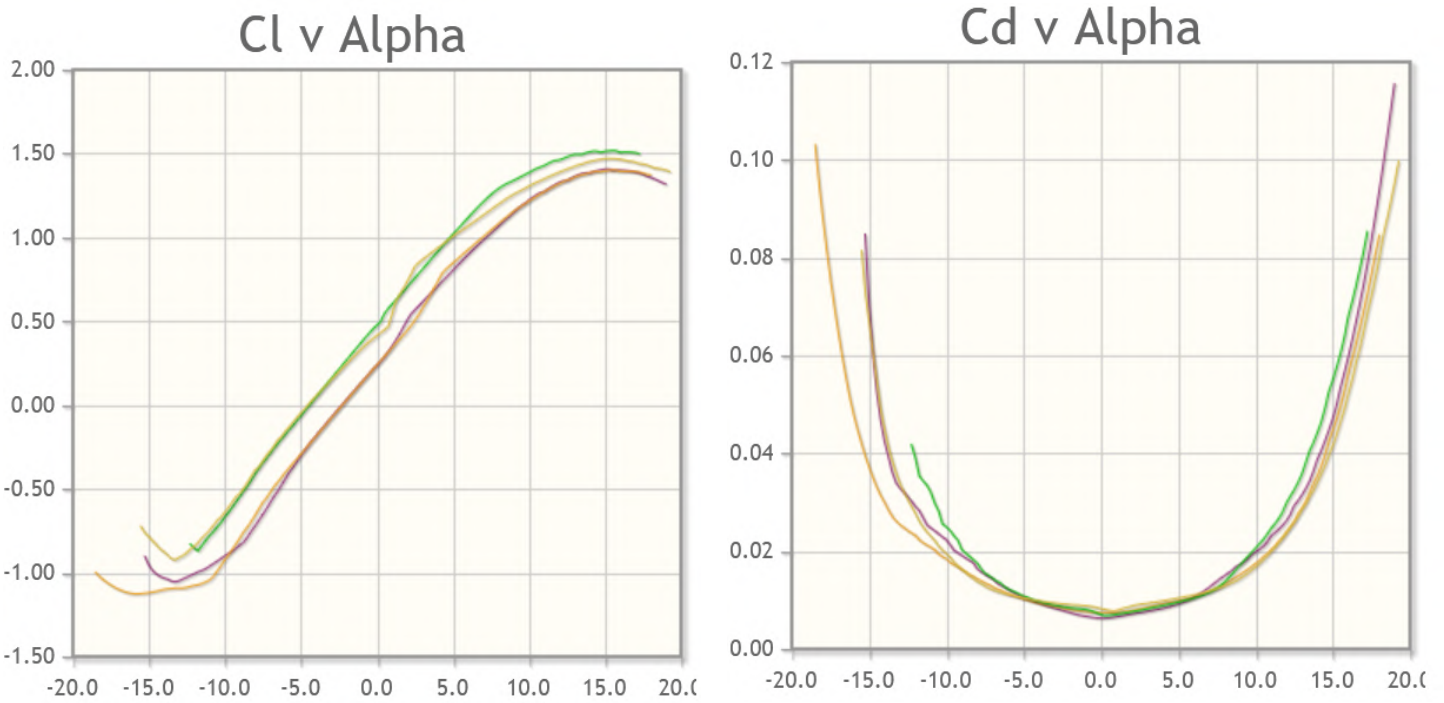


Figure 13: C_L and C_D vs. α plots for NACA 2412 (purple), NACA 4412 (green), NACA 2415 (orange), NACA 4415 (yellow)



The NACA 4412 airfoil was chosen because it provided a higher C_L than the other airfoils while maintaining a sufficient thickness to chord ratio to house electronics and carbon fiber spars.

4.2.2 Wing Sizing

In addition to constraints imposed by the rules, wing sizing was determined based on governing aerodynamic equations. The lift equation establishes a critical relationship between generated lift, velocity, and planform area. At cruise, lift equals weight, and the equation can be equivalently expressed as Eq. 6.

$$L = W = \frac{1}{2} \rho V^2 S_{REF} C_L \quad \text{Eq. 6}$$

A similar equation can be developed for drag where C_D can be expressed as a sum of the parasite drag coefficient and the induced drag coefficient, a function of C_L , AR, and e [2]:

$$D = \frac{1}{2} \rho V^2 S_{REF} C_D \quad \text{Eq. 7}$$

$$C_D = C_{D,parasite} + \frac{C_L^2}{\pi A Re} \quad \text{Eq. 8}$$

In this equation, e represents the Oswald efficiency factor, a scaling coefficient that characterizes the efficiency of the wing geometry. AR characterizes the span of the wing relative to its overall planform area, given by

$$AR = \frac{b^2}{S_{REF}}$$

Eq. 9

In order to determine wing sizing, an optimization program was developed in MATLAB that factored each of the above equations in addition to mission scoring to determine the parameters that returned the highest total mission score. The resulting aircraft had an aspect ratio of 4.62 with a total planform area of 1128 in². The resulting values of takeoff weight and cruise speed are included in Table 13.

Table 13: Wing Sizing Results

	M1	M2	M3
Planform Area [in²]	1128		
Aspect Ratio	4.6		
Takeoff Weight [lbs]	7	14	8
Cruise Speed [ft/s]	54.83	77.54	58.62

4.3 Tail Design

4.3.1 Airfoil Selection

For the horizontal stabilizer, the NACA 0010 airfoil was selected, while the vertical stabilizer uses the NACA 0008 airfoil. The low thickness-to-chord ratios of these airfoils minimize drag, while providing sufficient space to house servos and two carbon fiber spars.

4.3.2 Tail Sizing

The horizontal tail is designed as a non-lifting surface, with its primary role being to balance the pitching moment of the main wing and provide an adequate stability margin. The vertical stabilizer is designed to generate restoring yawing and rolling moments for directional stability and control.

Tail sizing and placement were initially determined with tail volume coefficients as defined in Equations 10 and 11. We chose coefficients of $V_H = 0.06$ for the horizontal tail and $V_V = 0.05$ for the vertical tail based on recommended values in Shaufele [3].

$$V_H = \frac{l_t \times S_H}{c \times S_{REF}}$$

Eq. 10

$$V_V = \frac{l_t \times S_V}{b \times S_{REF}}$$

Eq. 11

4.4 Propulsion

Using eCalc, a performance prediction software, a list of potential propulsion packages was generated for testing. These packages are a combination of motor, battery, propeller, and ESC which delivered sufficient thrust and endurance

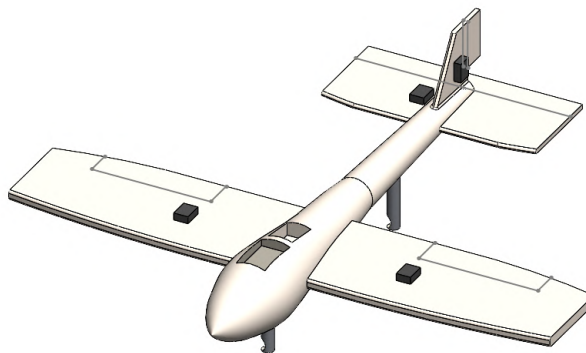
properties for M2 and M3. From the wing sizing and mission rules, the package(s) must be capable of achieving takeoff with the MTOW of 14 lbs for M2 and demonstrate an endurance of over 5 minutes for M3. Testing was performed to determine the package which could achieve the highest mission score.

4.5 X-1 Test Vehicle

In order to maximize total score, the X-1 vehicle was designed in order to have the least weight while still being able to land in the 2.5-point bonus box. To achieve this, the X-1 vehicle is a monoplane equipped with a rectangular wing, measuring 5 inches in chord and 22 inches in span. The wings incorporate a 5-degree upward dihedral angle to enhance self-stabilization, optimizing glide performance. The rectangular design further contributes to stability and efficient gliding by providing a uniform lift distribution and predictable aerodynamic behavior. Compared to tapered or swept wing configurations, which may introduce increased drag or instability at lower speeds, the rectangular configuration enhances stability.

The tail design of the X-1 vehicle features an inverted conventional tail configuration to ensure a flush connection with the main fuselage. This would allow for less parasitic drag on the entire aircraft as well as a more stable connection. Compared to T-tail or V-tail configurations, the inverted conventional tail minimizes interference with the main wing's airflow, reducing potential aerodynamic disturbances. Additionally, this design is easier to manufacture allowing the team to conduct more tests. The horizontal stabilizers have a chord length of 3.75 inches and a span of 9 inches, while the vertical stabilizer has a chord length 3.5 and span of 3 inches.

Figure 14: Preliminary Glider Design



4.4 Lift and Drag Predictions

4.4.1 Drag

To predict the drag of the aircraft, a built-up drag method, as outlined in Raymer [4], was applied and is represented by Eq. 12. In this method, parasite drag is calculated using the equivalent flat plate area (f) of each component of the aircraft given in Eq. 13. Drag is calculated using Eq. 8, where parasite drag is estimated using Eq. 12.

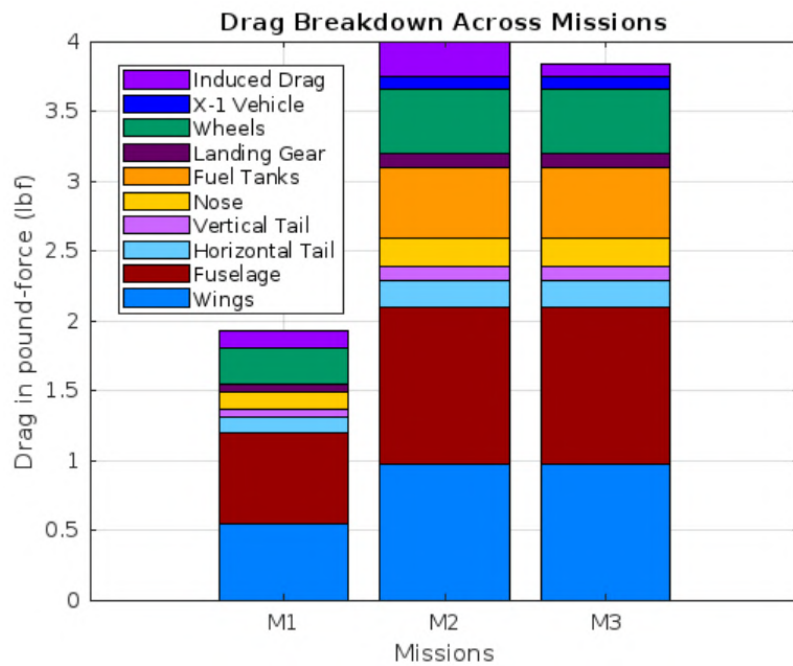
$$C_{D,\text{parasite}} = \frac{\Sigma f}{S_{REF}}$$
Eq. 12

$$f = \text{form factor} \times S_{WET} \times C_f$$
Eq. 13

Form factor and the skin friction coefficient C_f can be found graphically, while S_{WET} refers to the exposed surface area of each component.

To simplify calculations, a MATLAB program was designed to accept the aircraft geometry as an input and return the drag breakdown of the aircraft. Results are shown in Figure 15. The program was run for each mission configuration, and expected drag values were compared.

Figure 15: Drag Breakdown Across Missions



4.4.2 Lift

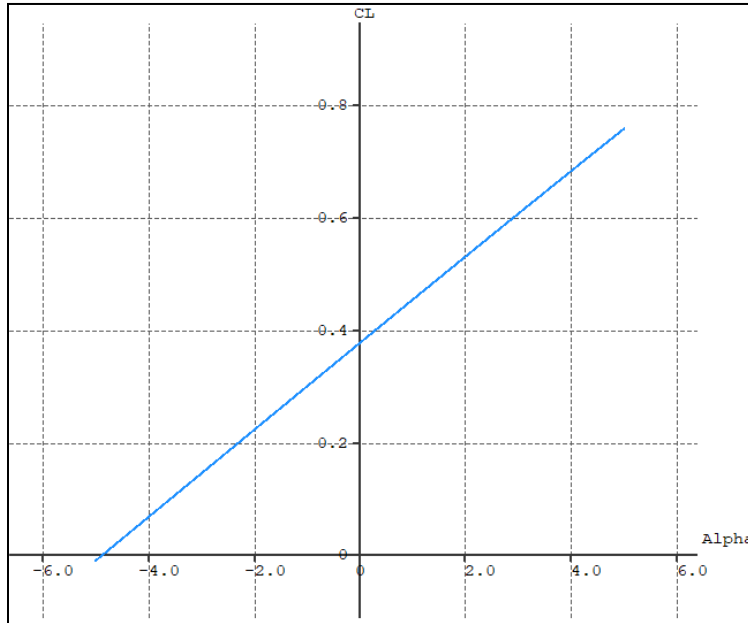
The minimum C_L in order to achieve steady flight at cruise for each mission was calculated from Eq. 6 using cruise speed and weight from wing sizing. Results are listed in Table 14.

Table 14: C_L at Cruise Speed by Mission

	M1	M2	M3
Cruise C_L	0.13	0.27	0.15
Cruise Speed [ft/s]	75	85	70
Weight [lbs]	6.135	13.91	7.03

To determine whether the lift produced was sufficient, XFLR5 was utilized to predict lift characteristics. Simulations of the rectangular wing planform were used to collect data on C_L , shown in Figure 16.

Figure 16: C_L vs. α for selected wing geometry



At moderate angles of attack, the aircraft successfully produced C_L values greater than the minimum, validating initial estimates.

4.5 Stability

4.5.1 Static Stability

To calculate the static margin, XFLR5 was used to determine the neutral point and center of gravity positions relative to the wing's leading edge. The stability analysis also extended to other critical parameters, including pitch moment coefficient, pitch damping, roll stability, yaw stability, and yaw damping. The static margin of 18.2% was then computed using Eq. 14.

$$SM = \frac{x_{NP} - x_{CG}}{\bar{c}}$$
Eq. 14

The neutral point was found to be 7.5 inches behind the wing's leading edge, the CG was 4.6 inches behind the leading edge, and the mean aerodynamic chord was derived from our wing geometry.

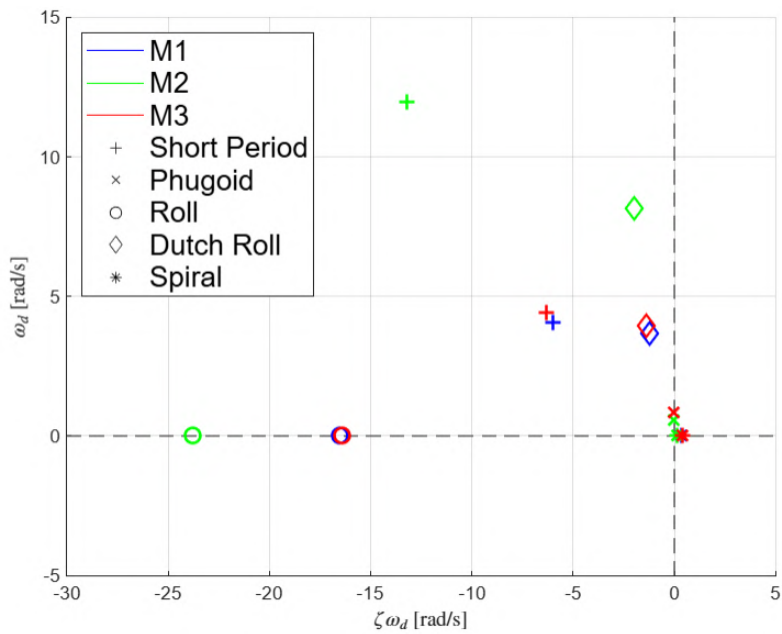
Table 15: Static Stability Constants

Type	$C_{M\alpha}$	C_{Mq}	$C_{I\beta}$	$C_{n\beta}$	C_{lr}	Static Margin
Recommended	-0.3 to -1.5	-5 to -40	< 0	0.05 to 0.4	-0.1 to -1	10% to 30%
Calculated	-0.8	-20	-1.0	0.2	-0.5	18.2%

4.5.2 Dynamic Stability

Dynamic stability, which refers to the ability to return to equilibrium over time, of our aircraft was analyzed using XFLR5. All five dynamic modes, which include short period, phugoid, roll, dutch roll, and spiral, were analyzed for all three missions. Root locus plots were used to determine the eigenvalues of the two longitudinal and two lateral modes, and these were plotted using MATLAB. If a mode's real component is negative, it means there is a decaying oscillation, which means it is stable. All modes of our aircraft are stable across all missions except for spiral mode. Spiral stability can be achieved through increasing the size of the vertical fin, having a dihedral, or a wing sweep, but these would increase drag, reduce the maneuverability, and create manufacturing complications. The pilot workload for managing this instability is low since the spiral mode has a slow and gradual divergence.

Figure 17: Root Locus Plot Of Dynamic Stability



For M1, our aircraft has Level 1 flying qualities, as described in MIL-F-8785C [5], for all modes except for the phugoid mode, which has the Level 2 qualities. For M2, our aircraft has the Level 1 flying qualities for all modes. This means the aircraft needs minimal input from the pilot to remain stable. These results are summarized in Table 16.

Table 16: Dynamic Stability Results

Mode	ζ			ω_d [rad/s]			$\zeta\omega_d$ [rad/s]			Time to Half Amplitude [s]		
	M1	M2	M3	M1	M2	M3	M1	M2	M3	M1	M2	M3
Short Period	0.830	0.738	0.812	4.028	11.97	4.420	-5.995	-13.08	-6.333	0.116	0.053	0.109
Phugoid	0.022	0.041	0.030	0.841	0.550	0.851	-0.019	-0.023	-0.026	36.87	30.54	26.87
Roll	-	-	-	-	-	-	-16.50	-23.76	-16.40	0.042	0.029	0.042
Dutch Roll	0.314	0.233	0.330	3.654	8.156	3.943	-1.210	-1.956	-1.376	0.573	0.354	0.504
Spiral	-	-	-	-	-	-	0.376	0.112	0.391	1.845	6.166	1.772

4.6 Predicted Mission Performance

Mission performance for the aircraft was predicted using the above equations, estimates, and simulations. Results are displayed in Table 17.

Table 17: Predicted Mission Performance

Parameter	M1	M2	M3
Takeoff Weight [lb]	7	14	8
TOFL [ft]	11.27	19.61	16.40
Cruise C_L	0.13	0.27	0.15
Cruise Speed [ft/s]	75	80	75
Cruise L/D	8.9	14.7	9.7
Stall Speed [ft/s]	21.7	30.65	23.17
Payload [lbs]	-	7	-
Number of Laps	3	3	6
Mission Time [s]	135	150	280

4.7 Uncertainties

Many simplifications are made throughout in order to generate a preliminary estimation of AnteAir's performance. In particular, the assumptions made to develop equations for lift, drag, and other flight characteristics are based on multiple simplifications in order to simulate flight given limited computational power. Initial assumptions are made for critical

parameters such as thrust or cruise speed based on previous years and are refined through reiteration and testing. Calculations also rely on standard atmospheric conditions, which may not reflect the actual conditions of Tucson, Arizona.

5. Detail Design

5.1 Dimension Table

Table 18 summarizes the dimensions of the aircraft and propulsion package.

Table 18: Dimension Table

Wing		Tail	Horizontal	Vertical
Airfoil	NACA 4412	Airfoil	NACA 0010	NACA 0008
Span [in]	72	Span [in]	30	11
MAC [in]	15.60	Chord [in]	10	
Wing Area [in ²]	1128	Surface area [in ²]	572.20	223.76
Aspect Ratio	4.62	Platform Area [in ²]	280	110
Incidence Angle	2°	Aspect ratio	3	1.1
Static Margin	18.2%	Incidence Angle [deg]	0°	0°
Propulsion		Tail Arm [in]	35	35
Battery	Tattu 4500mAh 6s 25C 22.2V LiPo	Fuselage		
Motor	SunnySky X4130-8 380 KV	Total Length [in]	57.25	
ESC	Castle Creations Phoenix Edge Lite 100 Brushless ESC Speed Control w/ 5-Amp BEC	Storage Length [in]	36.13	
Propeller	18 x 10E	Tail Length [in]	11.63	
Receiver	Futaba R7008SB Receiver	Width [in]	4.5	
Servos	Futaba S-AG300 S.Bus2 HV Narrow Airplane Serv	Height [in]	4.5	

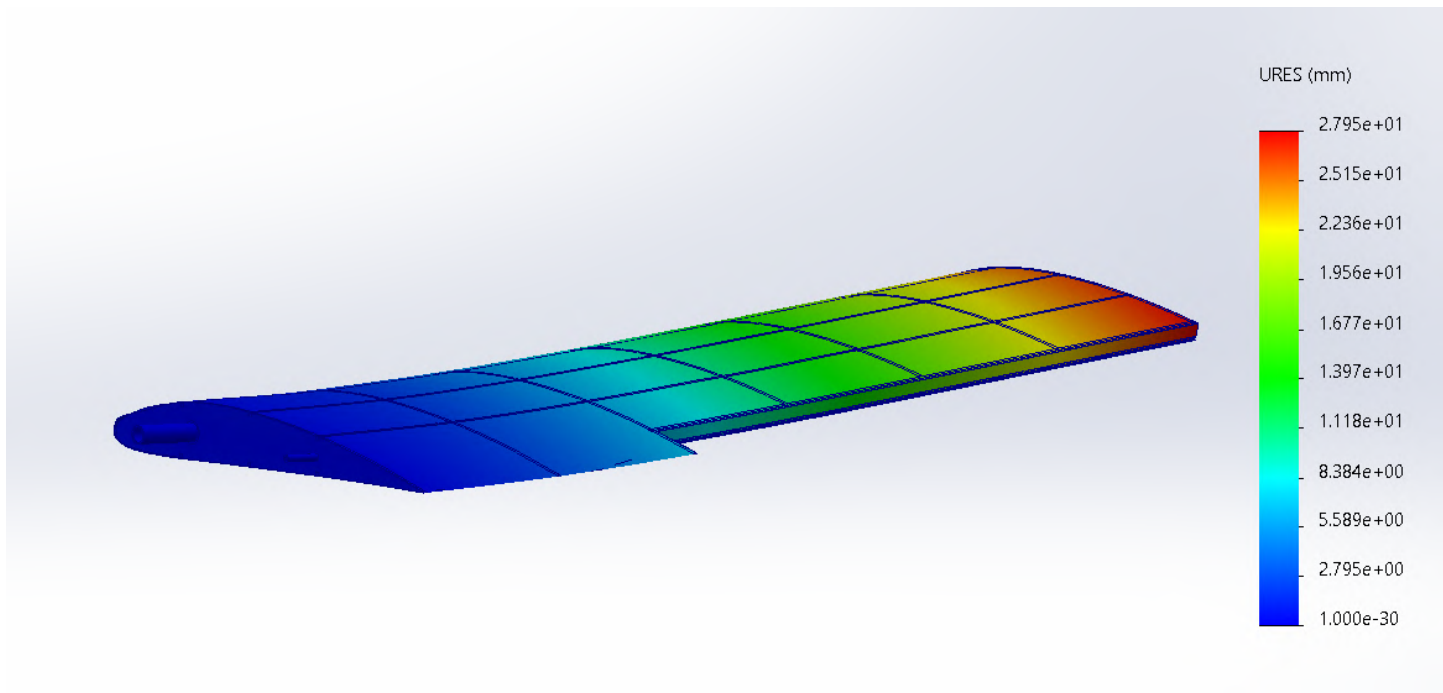
5.2 Structural Capabilities

In order to successfully meet predicted mission performance, the aircraft structure must be capable of withstanding loads at the MTOW of 13.91 lbs. During high-stress maneuvers such as turns, the aircraft can experience a load factor of up to 3Gs. To predict the structural capabilities of our aircraft, simulations were conducted on the primary structural elements.

5.2.1 Wing

The wing consists of a balsa-built-up structure reinforced by a carbon fiber main and rear spar. With the root fixed, a load of 35 lbf was applied to the wingtip to simulate a wing load of 2.5 Gs. The wing experienced a maximum deflection of 0.11 in, or 0.31% of the half-span of the wing.

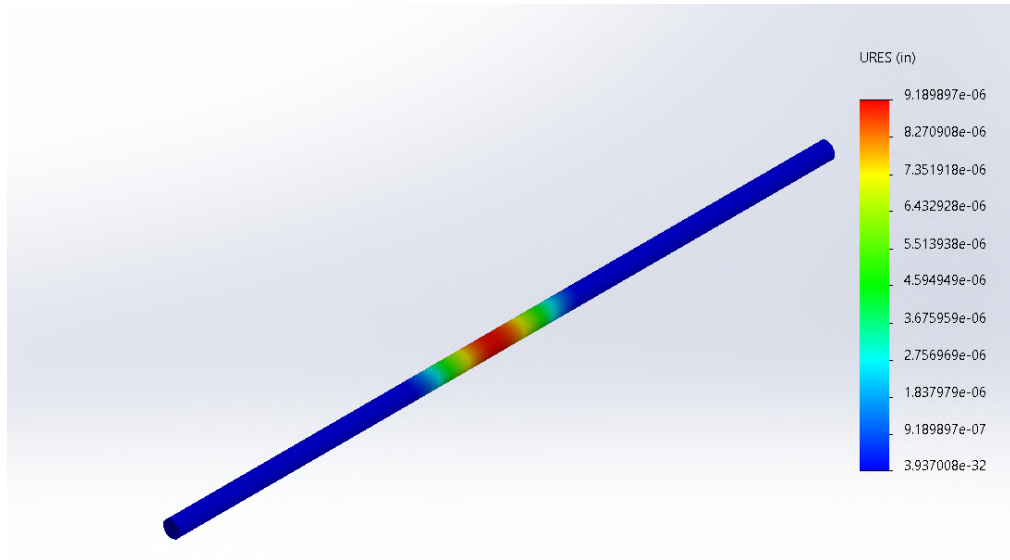
Figure 18: Wing FEA Analysis Results



5.2.2 Fuselage Boom

The main structural component of the fuselage is a carbon fiber spar with an outer diameter of 0.76" and inner diameter of 0.625". Applying a load of 3 Gs at the center of lift resulted in minimal deflection.

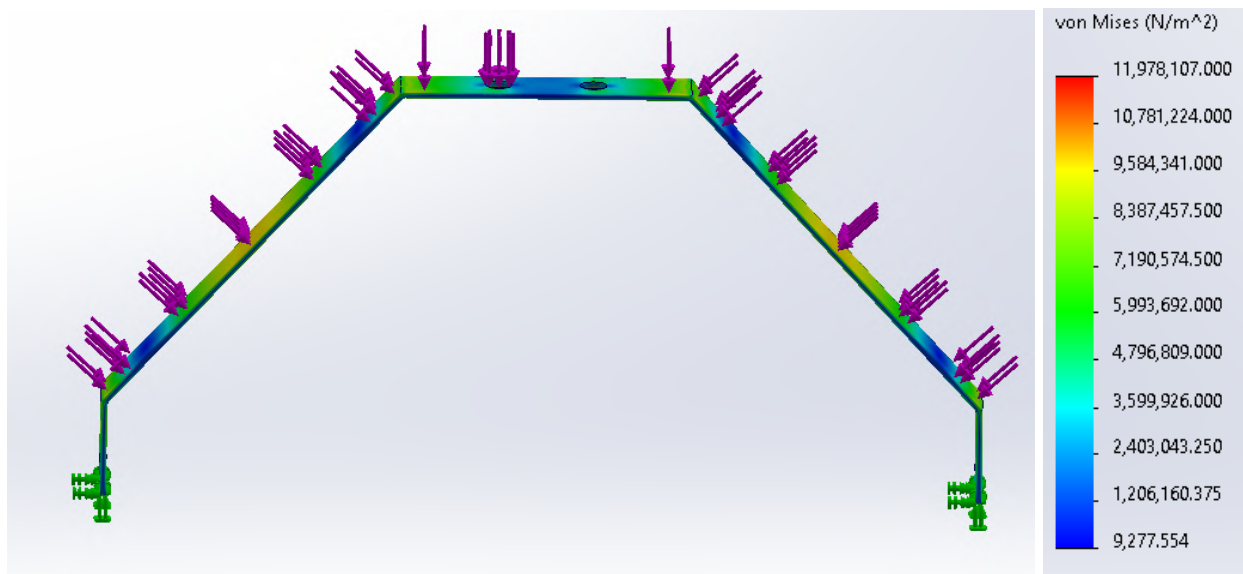
Figure 19: Fuselage Boom FEA Analysis Results



5.2.3 Landing Gear

The landing gear is a carbon fiber composite structure designed to withstand forces at landing impact. An FEA analysis, shown in Figure 20, was conducted in SolidWorks to test the structural integrity of the landing gear. A static test was performed with a weight of 20 lbs, approximately 150% of the MTOW. The maximum stress experienced was 250,167 lbf/m², significantly less than the elastic modulus of 1,151,00 lbf/m². No damage or permanent deformation was expected.

Figure 20: Landing Gear FEA Analysis results



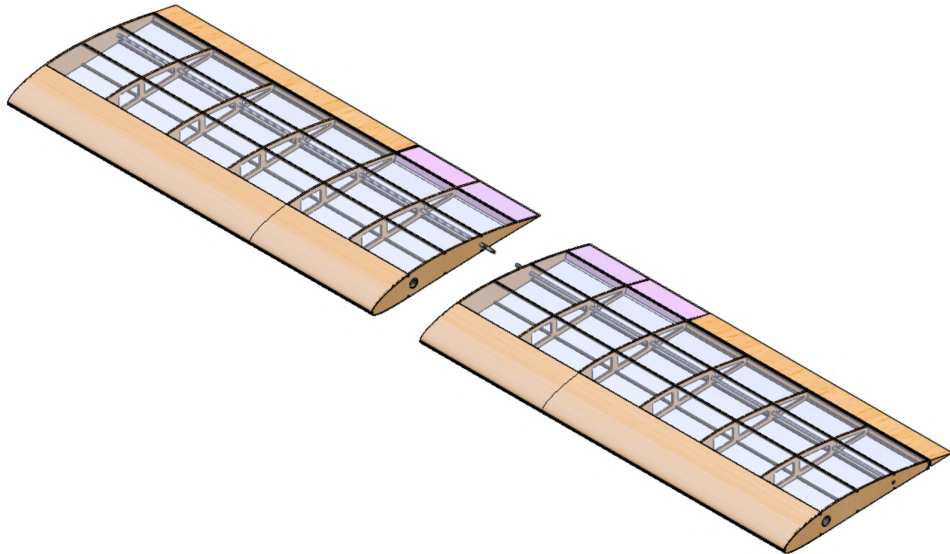
5.3 Subsystem Design

5.3.1 Wing

The two wing sections are constructed using a built-up balsa structure consisting of spaced balsa ribs attached to a main and rear carbon fiber spar. The main spar has an OD of 0.76" and is placed at quarter-chord to resist lift-induced bending

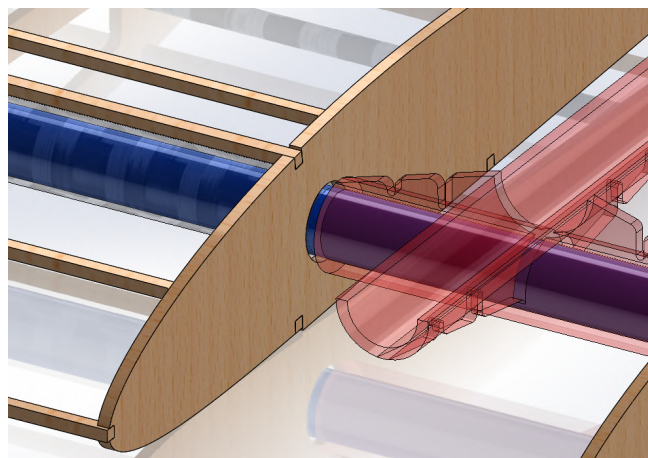
moments. The rear spar has an OD of 0.285" to resist wing twist. Stringers run along the span of the wing and the leading edge is covered with a 1/32" layer of balsa sheeting to provide a smooth surface for a layer of monokote. The trailing edge of the inboard ribs are reinforced with insulation foam to maintain the shape of the wing. The ailerons are attached using Blenders and actuated using servos attached to the ribs. The complete structure is shown in Figure 21.

Figure 21: Wing Structure



To connect the wings to the fuselage, a ferrule is inserted into the main and rear spars of the wing and attached to a 3D-printed bracket in the fuselage as shown in Figure 22. The wings are held together by a releasable zip tie for easy detachment.

Figure 22: Wing Connection

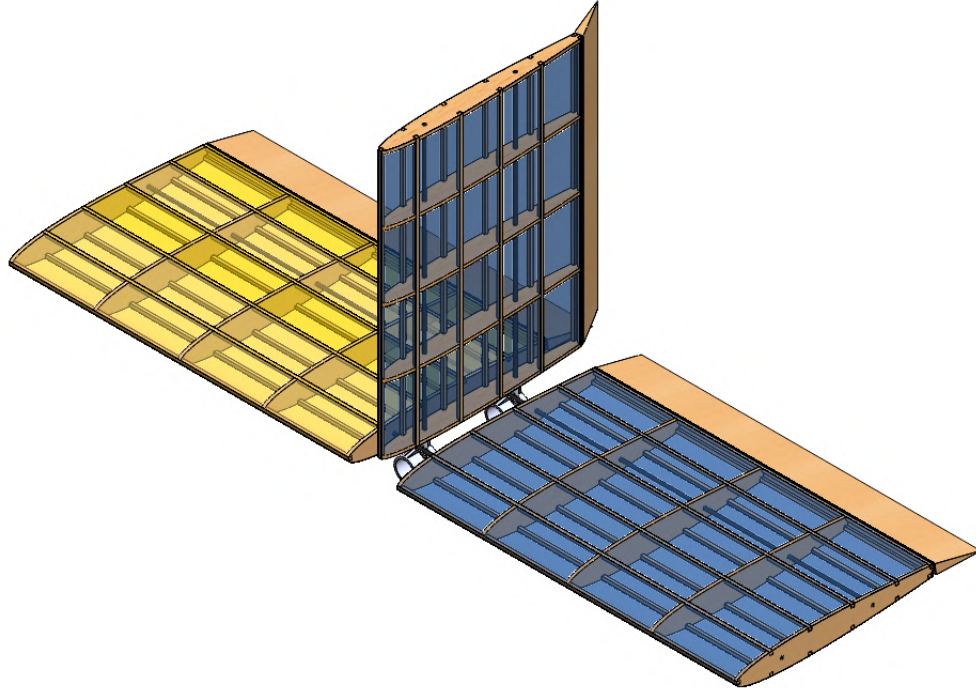


5.3.2 Empennage

The empennage is shown in Figure 23. Both the horizontal and vertical tails are constructed using a built-up balsa structure reinforced with carbon fiber rods. The two rods provide resistance against bending and twisting. The rods are inserted into a 3D printed connection and epoxied to the boom. Stringers run along the span and the surface is

monokoted. The elevator and rudder run along the entire length of the tails and are attached using Blenderm. The surfaces are actuated using servos mounted in the ribs.

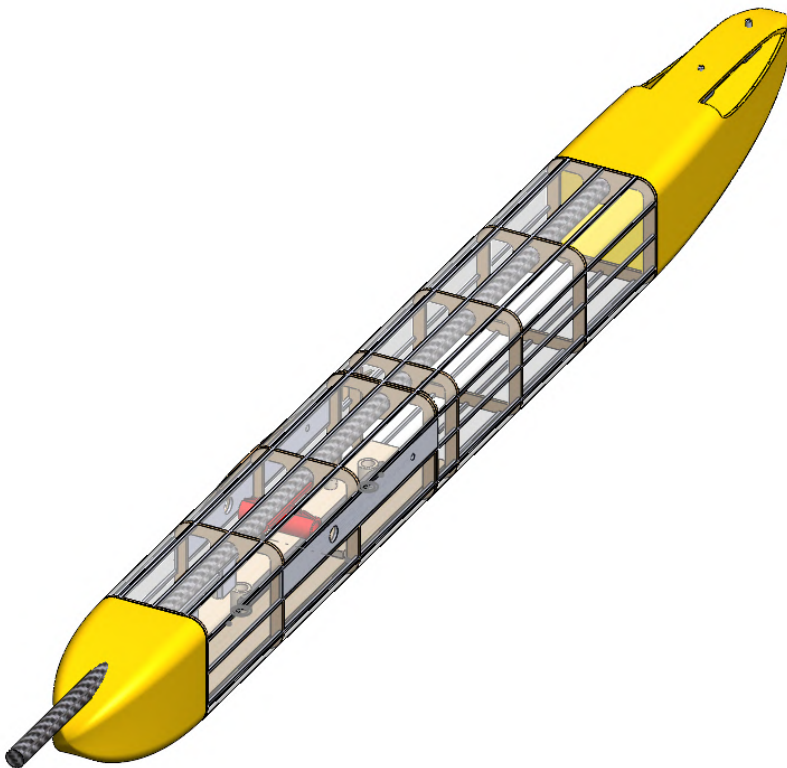
Figure 23: Empennage Structure



5.3.3 Fuselage

The fuselage is a series of plywood and balsa bulkheads supported by a 0.76" OD carbon fiber boom. Stringers run along the length of the fuselage to provide a frame for monokote. Bulkhead spacing is determined by structural demands, with more support at the landing gears and wing mounting location. A plywood floor runs along the bottom of the fuselage, with cutouts to mount the glider attachment mechanism. The nose and tail cone are constructed using foam board and assume an elliptical profile to minimize drag. The fuselage is shown in Figure 24.

Figure 24: Fuselage Structure



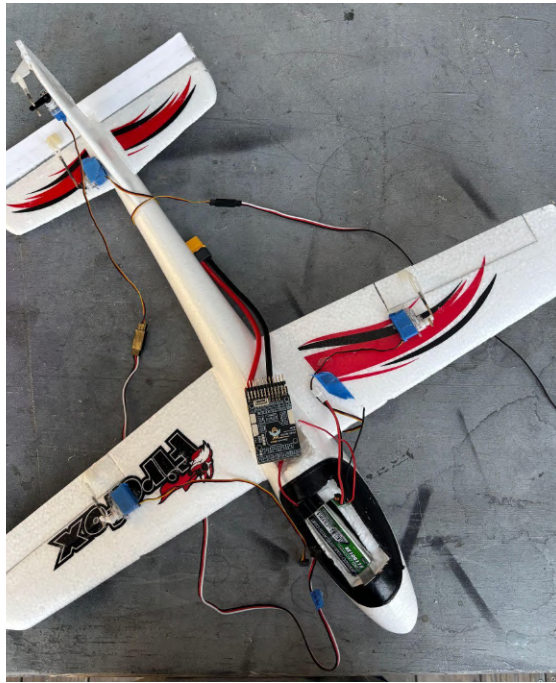
5.3.4 X-1 Test Vehicle

Following an evaluation of previous and working airfoil designs, a flat plate airfoil was selected for both the wings and tails. At the low Reynolds numbers characteristic of the X-1 test vehicle's flight regime, the flat-plate airfoil demonstrated superior performance in terms of glidability and controllability compared to traditional airfoils. Traditional airfoils often experience flow separation and increased drag in low-speed, small-scale applications. However, flat-plate airfoils maintain a more stable and predictable flow profile, reducing drag and enhancing maneuverability, making them particularly effective for lightweight gliders operating at low speeds. The lifting surfaces of the X-1 test vehicle have been dimensioned to carry the onboard electronic package.

The X-1 test vehicle is equipped with a Speedybee F405 Wing Mini (0.051 Lbs) flight controller as well as a GPS in order to land in the 2.5-point bonus box. This controller was chosen over other flight controllers like the Matek F405 Wing-V2 (0.55 Lbs) and the Pixhawk 6c Mini (0.086 Lbs) due to the ease of use as well as being the lightest of the group. The Speedybee controls 4 different HS-40 Servos in order to move the ailerons, elevator, and rudder.

The battery selection for the X-1 test vehicle was critical to maintaining its weight below the 0.55-pound limit. To achieve this, the X-1 test vehicle utilizes a 3.7V battery weighing just 0.039 pounds, paired with a step-up converter weighing 0.002 pounds. This combination keeps the vehicle lightweight, as the electronics require minimal power draw. However, a 5V battery, which typically weighs around 0.3 pounds, would demand a higher weight allocation, resulting in a lower score. By using the 3.7V battery and step-up converter, with a total weight of only 0.042 pounds, the X-1 test vehicle optimizes both performance and efficiency. The test vehicle is shown in Figure 25.

Figure 25: X-1 Test Vehicle With Electronics



The step-up converter advertises an 80-93% conversion rate, with calculations below assuming the minimal efficiency of 80% to simulate a worst-case scenario battery draw for the electronic system. A step-up converter is necessary because the selected flight controller requires a 5V input, which a 3.7V battery cannot provide without conversion. The calculations shown in Figure 26 illustrate the projected battery draw for M3 to ensure the battery has sufficient amperage to power the X-1 test vehicle. The electronics are assumed to operate at running draw for the entire descent, providing a conservative overestimation of energy usage, as not all servos will be at maximum draw at all times. The total battery capacity in mAh is also calculated, including the conversion from 3.7V to 5V and the corresponding efficiency loss due to the step-up converter.

Figure 26: X-1 Test Vehicle Calculations

$$\text{Servo running draw} = 460 \text{ mA} \times \frac{\frac{1 \text{ hour}}{60 \text{ minutes}}}{\text{ }} \times 6 \text{ minutes} = 46 \text{ mAh}$$

$$\text{Total servo running draw} = 46 \text{ mAh} \times 4 \text{ servos} = 184 \text{ mAh}$$

Speedybee running draw: 400 mA

$$6 \text{ minutes} \times \frac{\frac{1 \text{ hour}}{60 \text{ minutes}}}{\text{ }} \times 400 \text{ mA} = 40 \text{ mAh}$$

$$\Sigma \text{ Power Draw} = 184 + 46 = 230 \text{ mAh}$$

Battery selected: 3.7 Volt 500 mAh battery

$$500 \text{ mAh} \times 3.7 \text{ Volt} \times \frac{\frac{1 \text{ mAh}}{1000 \text{ Ah}}}{\text{ }} = 1.85 \text{ Watt hours}$$

$$\text{Capacity at 5 volts} = \frac{\text{Energy (Wh)}}{\text{Volts}} = \frac{1.85}{5} \times \frac{1000 \text{ Ah}}{1 \text{ mAh}} = 370 \text{ mAh}$$

To show maximum potential loss due to step up converter,

$$\text{Capacity}_{\text{real}} = \text{Capacity}_{\text{ideal}} \times 0.8 = 370 \text{ mAh} \times 0.8 = 296 \text{ mAh}$$

Battery holds 296 mAh, electronics use 230 mAh

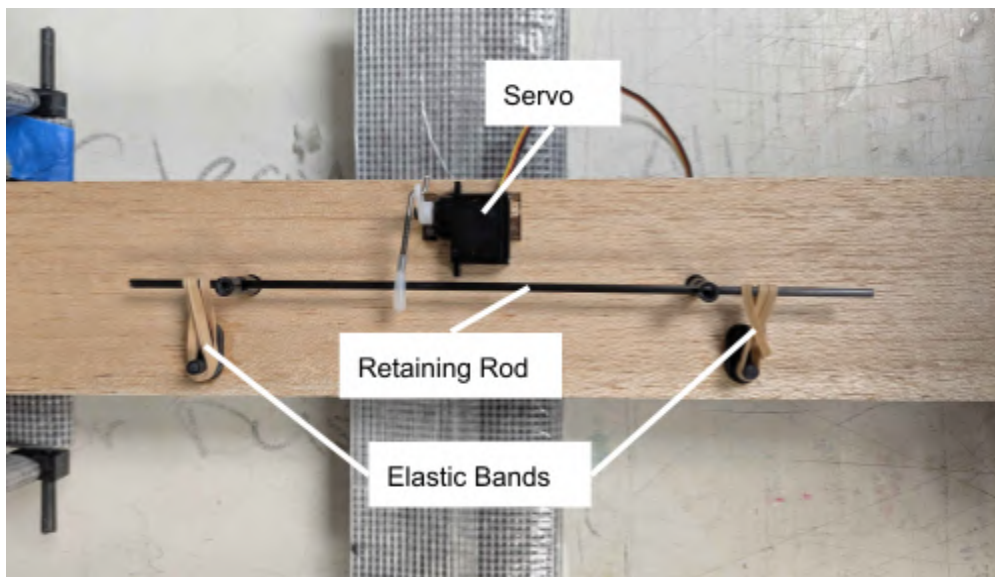
To activate the blinking LED when the X-1 test Vehicle detaches from the airplane, a breakwire design was created. The circuit has two parallel paths connected to a battery. One path contains a wire that gets bridged by the conductive part of our attachment mechanism, while the other path contains a resistor and a blinking LED. When the X-1 test vehicle is attached to the plane, that conductive connection bridges the wire gap, completing the first path and creating a short circuit that keeps the LED off. When the X-1 test vehicle detaches, the conductive connection breaks, opening that first path and letting current flow through the LED path instead, which causes the light to start blinking. This gives us a clear visual signal that the X-1 test vehicle has successfully separated.

The X-1 test vehicle operates with the INAV 6.1 flight control software running on a Speedybee controller to manage the flight control system. The choice between INAV and alternatives like ArduPilot came down to a few key factors. INAV needs significantly fewer computing resources, using only 150 KB ROM and 32 KB RAM compared to ArduPilot's 350 KB ROM and 64 KB RAM requirements. This was crucial working with the limited capabilities of the Speedybee controller's STM32F4 processor. INAV's control loop runs at 500 Hz, giving a quick response time needed for stable flight control. One of INAV's strongest features for our application is its built-in waypoint navigation system. Since the exact flight path the airplane will take is known as well as the location of our landing zone. Pre-programmed waypoints can be put into INAV's mission planner. This allows a defined flight path, including the estimated deployment point, turn initiation point, and landing approach trajectory. INAV's navigation system automatically handles the transition between waypoints while maintaining stable flight, and includes built-in safety features like minimum altitude restrictions and geo-fencing.

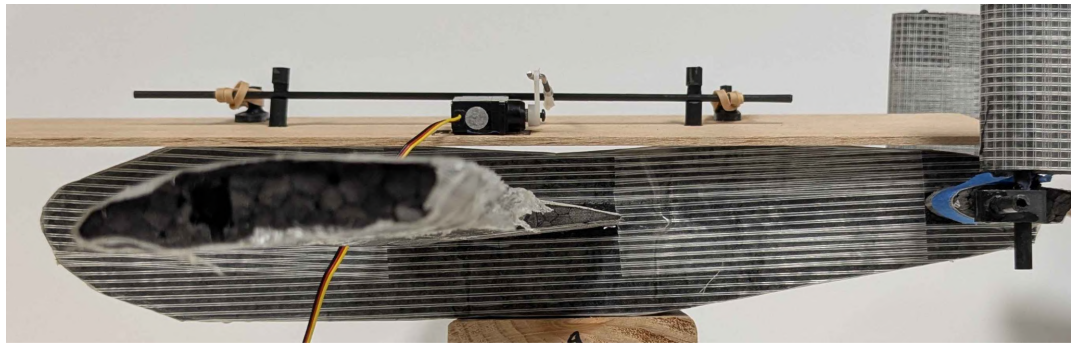
5.3.5 X-1 Test Vehicle Attachment

The X-1 test vehicle is attached by a retaining rod held in place by two elastic bands. When the servo is actuated, the retaining rod is released, and the vehicle is dropped from the aircraft. The mechanism, attached to an early prototype of the X-1 test vehicle, is shown in Figure 27.

Figure 27: X-1 Test Vehicle Attachment on Prototype



(a) Top View

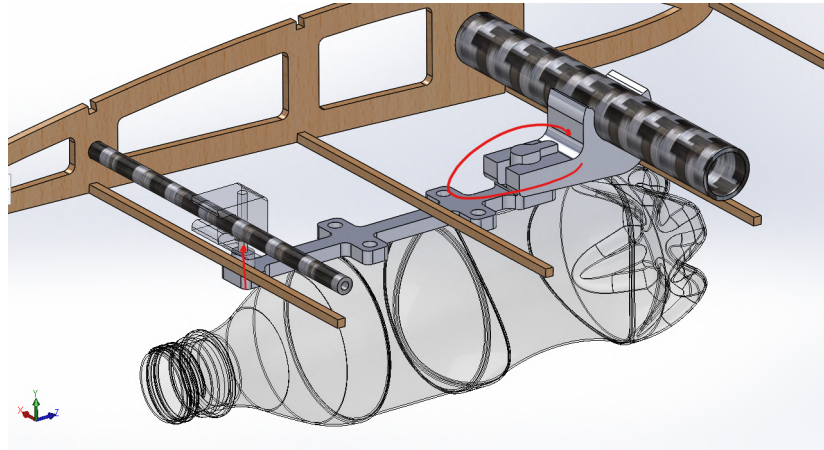


(b) Side View

5.3.6 Fuel Tank Attachment

The fuel tank attachment, pictured in Figure 28, utilizes a locking pin design for quick and reliable bottle attachment and detachment. Two 3D-printed connections are epoxied to the main and rear spar. The bottle and pylon are slid into a receiving 3D-printed slot on the main spar, with the bottle initially backward (cap pointing towards the aircraft's nose). The pylon is then rotated about the pin into its final orientation and a M4 thumb screw is inserted into the rear attachment to stop the bottle attachment from rotating during flight.

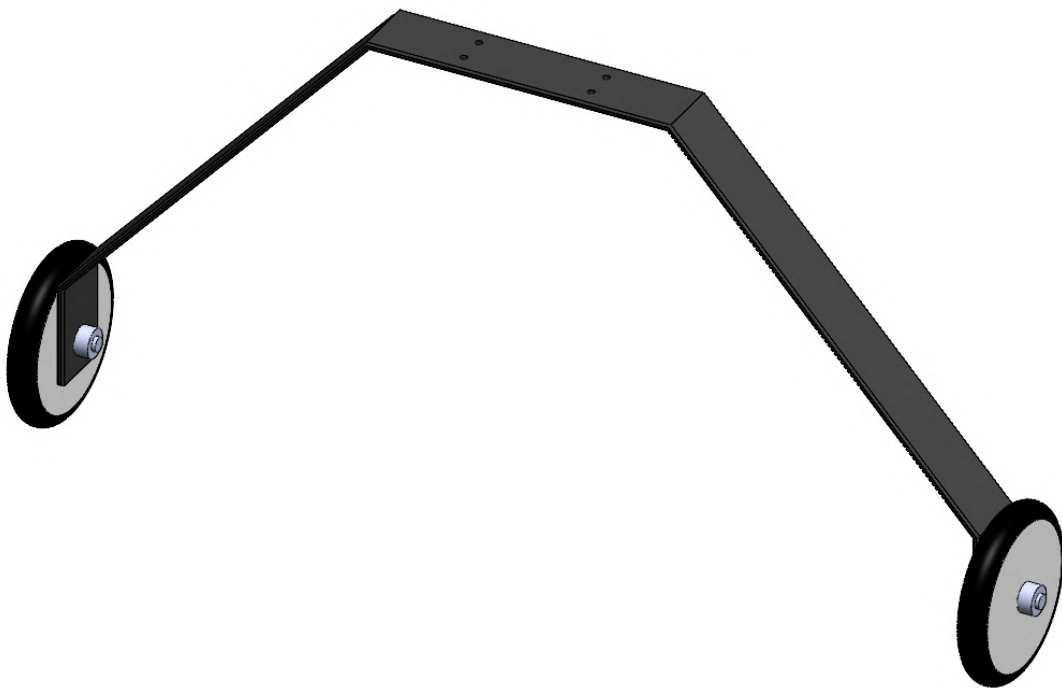
Figure 28: Bottle Attachment Mechanism



5.3.7 Landing Gear

The landing gear is screwed directly into the floor of the fuselage through four holes on the upper surface. The gear is attached between two thinly-spaced bulkheads to provide structural support and direct the load to the boom. Wheels are attached by small carbon fiber rods with end caps. The assembly is shown in Figure 29.

Figure 29: Landing Gear



5.3.8 Motor Mount

The motor is attached by screwing the X-plate into a 3D-printed mount, which is then wrapped in kevlar and epoxied to the boom. Simulations and testing ensure the mount remains affixed and sustains no structural damage during operation. The mount is shown in Figure 30.

Figure 30: Motor Mount

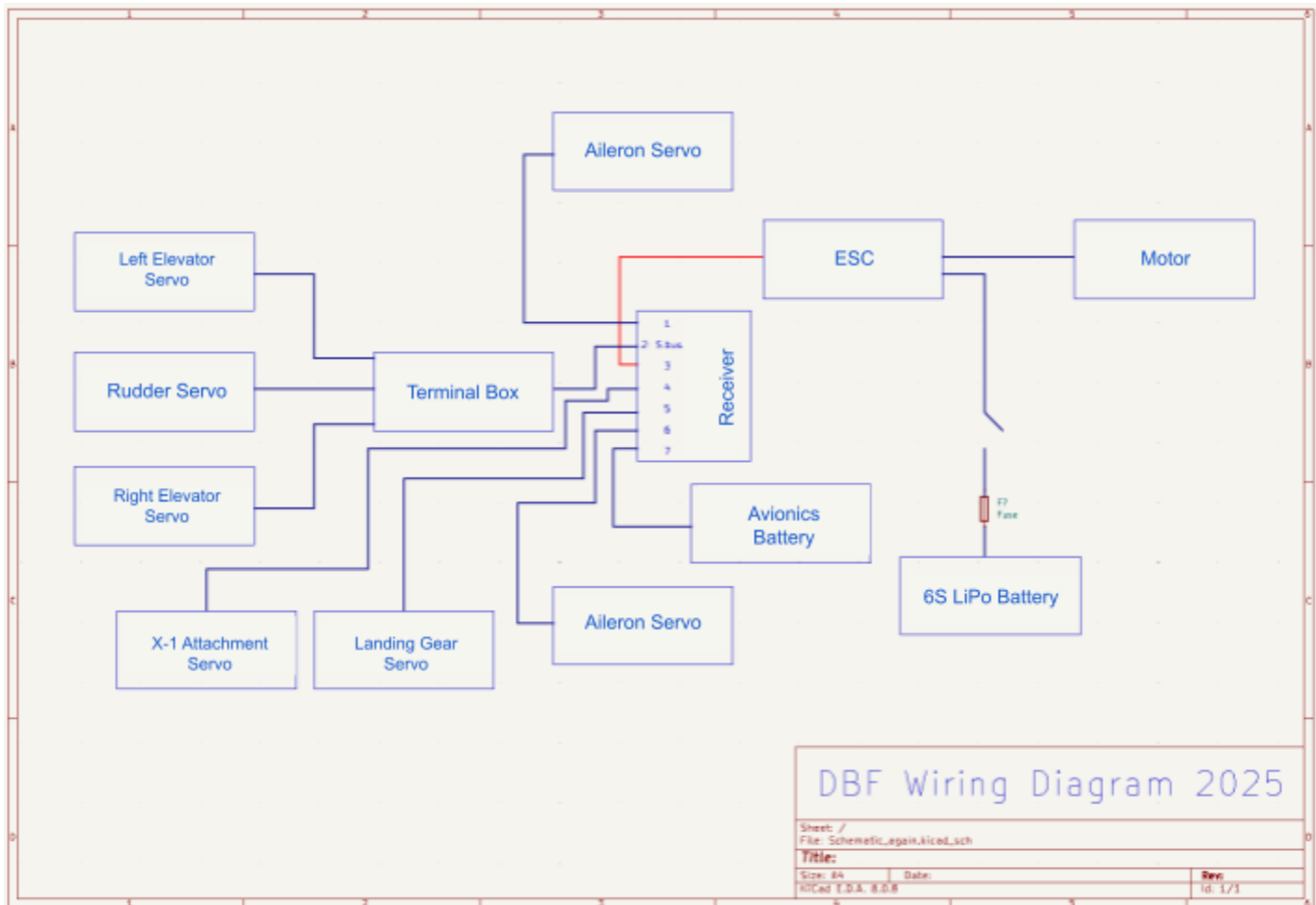


5.3.9 Wiring Diagram

The wiring diagram is shown in Figure 31. The avionics battery, aileron servos, landing gear servo, and glider servo connect directly to the receiver. Tail servos are connected to an SBUS terminal box, allowing control of each servo using a

single port on the receiver. The motor is connected to the ESC, which is controlled by the receiver and delivers power from the battery to the motor.

Figure 31: Wiring Diagram



5.4 Weight and Balance

The weight and balance data for the X-1 test vehicle and aircraft are shown in Tables 19 and 20. Weight is taken with reference to 1 inch in front of the central hub of the propeller. Changes in CG due to the addition of the fuel tanks and the X-1 test vehicle in M2 and M3 are counterbalanced by the change in position of the battery.

Table 19: X-1 Test Vehicle Weight Table

Component	Weight [lbs]	Component	Weight [lbs]
3.7 V Battery	0.039	Tails	0.015
Step Converter	0.002	Wings	0.035
Speedy Bee F405 Wing Mini	0.051	Other (Wires, Servo Horns, etc.)	0.03
GPS	0.025	Fuselage	0.065
HS40 Featherweight Servo X4	0.055	GPS	0.025
Total	0.317		

Table 20: Aircraft Weight Table

Component	Weight [lbs]	CG(x) [in]	CG(z) [in]	Component	Weight [lbs]	CG(x) [in]	CG(z) [in]
Wing	1.42	21.00	-2.00				Mission 1
Horizontal Tail	0.13	36.00	0.00	Propulsion Battery	1.33	18.00	-3.00
Vertical Tail	0.10	36.00	5.00	M1 Total	6.135	20.06	-1.85
Fuselage	1.24	36.00	-2.00				Mission 2
Main Gear	0.16	30.00	-7.00	Propulsion Battery	1.33	15.00	-3.00
Nose Gear	0.14	14.00	-8.00	X-1 Test Vehicle	0.32	26.00	-5.00
Propeller	0.17	1.00	0.00	X-1 Attachment	0.12	26.00	-5.00
Motor	1.02	2.00	0.00	Pylons	0.20	22.00	-1.00
ESC	0.24	10.00	1.00	Fuel Tanks	7.00	22.00	-4.00
Receiver	0.03	22.00	-3.00	M2 Total	15.08	21.02	-3.05
Avionics Battery	0.16	28.00	-3.00				Mission 3
				Propulsion Battery	1.33	18.00	-3.00
				X-1 Test Vehicle	0.32	26.00	-5.00
				X-1 Attachment	0.12	26.00	-5.00
				Pylons	0.20	22.00	-1.00
				Fuel Tanks	0.12	22.00	-4.00
				M3 Total	6.90	20.63	-2.12

5.5 Flight and Mission Performance

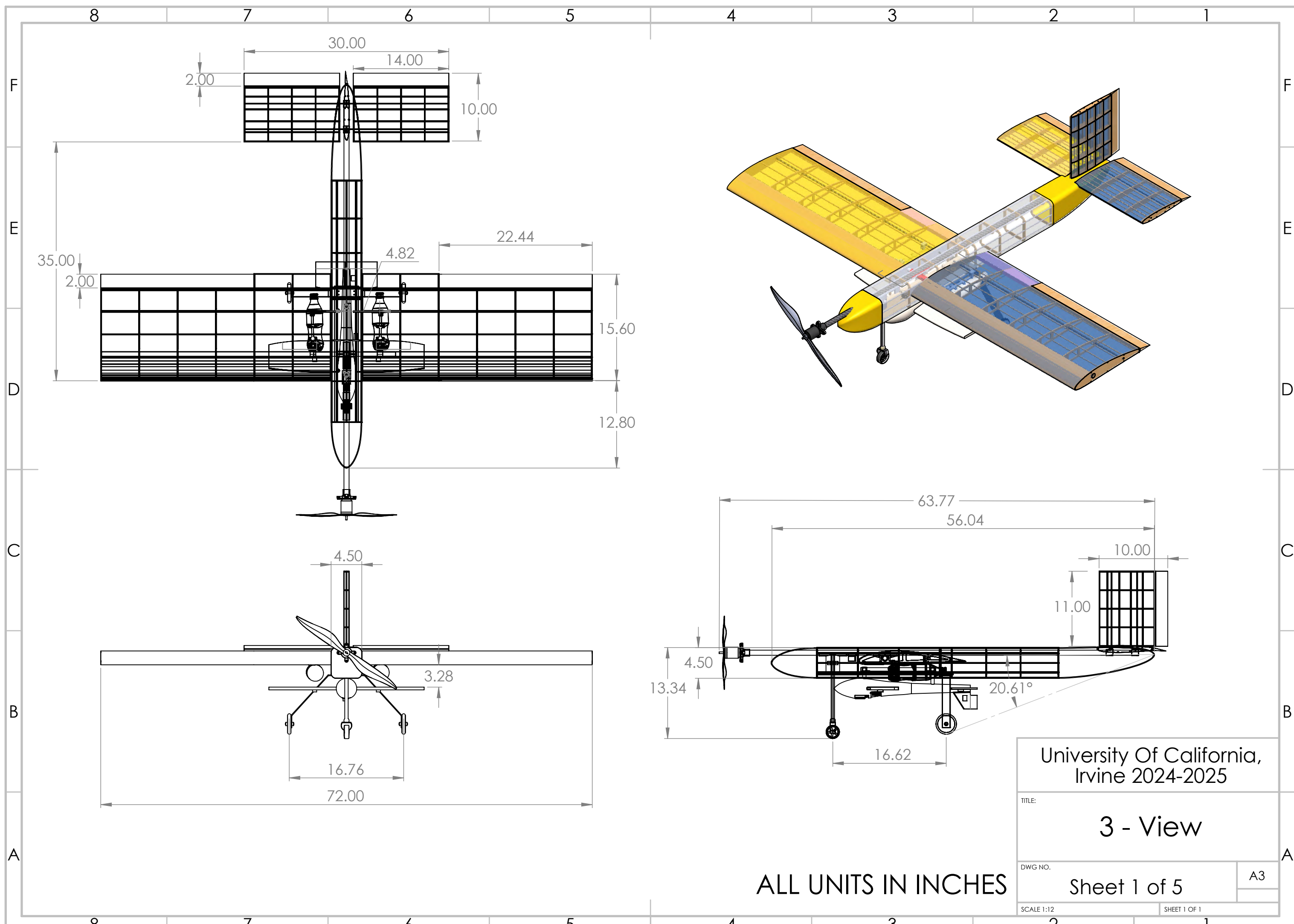
The predicted performance of *AnteetAir* is summarized in Table 21. Flight parameters were calculated by using values from collected data, resulting in a more accurate prediction of performance.

Table 21: Predicted Performance

Parameter	M1	M2	M3	GM
Takeoff Weight [lb]	6.135	13.91	7.03	-
TOFL [ft]	9.42	21.04	14.83	-
Cruise C_L	0.12	0.21	0.15	-
Cruise Speed [ft/s]	74.09	84.33	70.94	-
Cruise L/D	7.90	12.67	9.54	-
Stall Speed [ft/s]	20.29	30.55	21.72	-
Payload [lbs]	-	7	-	-
Number of Laps	3	3	5	-
Mission Time [s]	161.97	142.30	281.93	70
Predicted Score	1.00	1.47	2.65	0.29

5.6 Drawing Package

The following section contains a three-view drawing, a structural arrangement, and mission configurations for the aircraft, as well as an X-1 Test Vehicle three-view drawing and X-1 Test Vehicle structural arrangement. Drawings were created using SolidWorks.



SOLIDWORKS Educational Product. For Instructional Use Only.

ALL UNITS IN INCHES

University Of California, Irvine 2024-2025

TITLE

3 - View

1

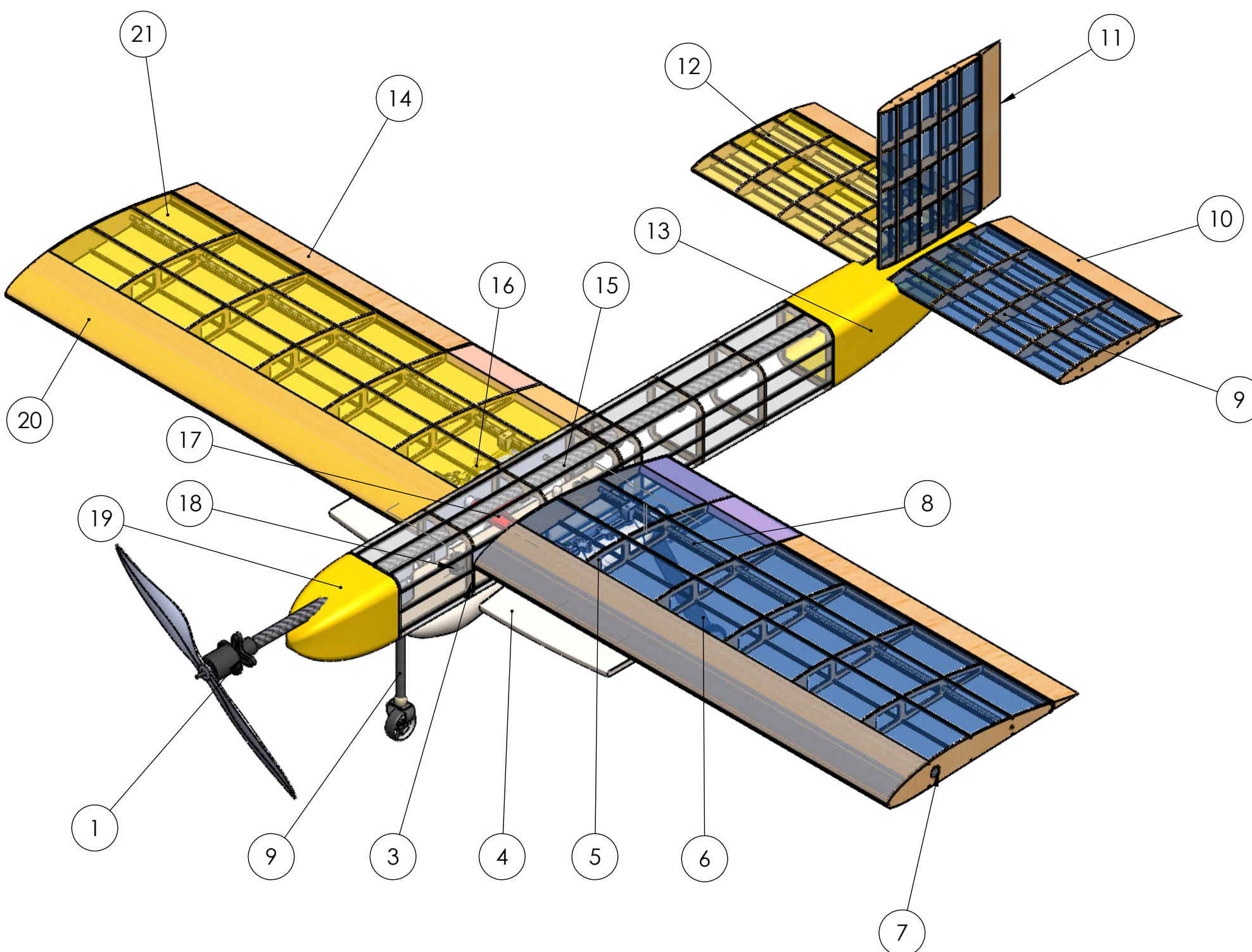
Sheet 1 of 5

A3

SHEET 1 OF 1

PAGE 1 OF 1

ITEM NO.	Description	Material	QTY.
1	Motor Mount	PLA Plastic	1
2	Nose Landing Gear	Carbon Fiber & Foam Wheel	1
3	Fuselage Bulkhead	Ply & Balsa Wood	1
4	X-1 Test Vehicle	EPO Foam	1
5	Wing Rib	Balsa Wood	14
6	Main Landing Gear	Carbon Fiber & Foam Wheels	1
7	Main Wing Spar	Carbon Fiber	2
8	Rear Wing Spar	Carbon Fiber	2
9	Tail Rib	Balsa Wood	15
10	Elevator	Balsa Wood	2
11	Rudder	Balsa Wood	1
12	Tail Spar	Carbon Fiber	4
13	Tail Cone	Foam Board	1
14	Aileron	Balsa Wood	2
15	Fuselage Boom	Carbon Fiber	1
16	Fuel Tank Attachment	PLA Plastic	2
17	Wing Connector	PLA Plastic	1
18	X-1 Test Vehicle Attachment	Carbon Fiber, Plywood	1
19	Nose Cone	Foam Board	1
20	Wing Sheeting	Balsa Wood	2
21	Monokote	Monokote Plastic	8



University Of California,
Irvine 2024-2025

Structure
Arrangement

TITLE:
DWG NO.
SCALE 1:7
Sheet 2 of 5
A3
SHEET 1 OF 1

8

7

6

5

4

3

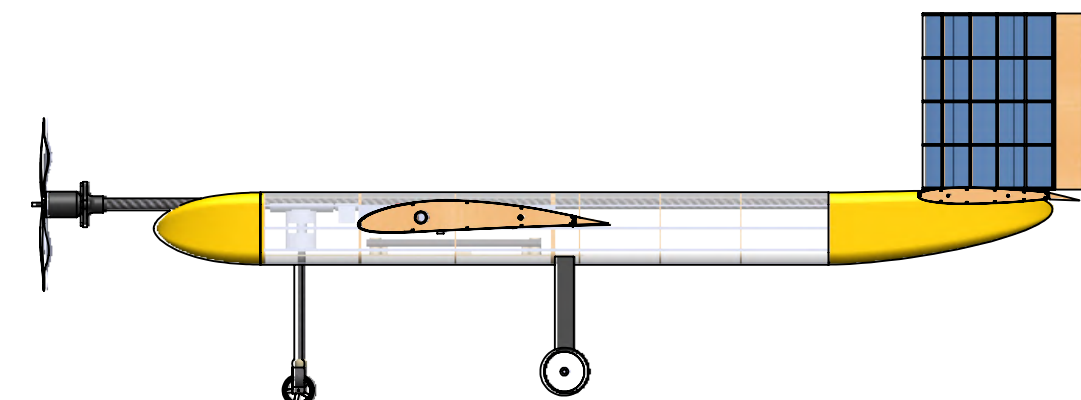
2

1

F

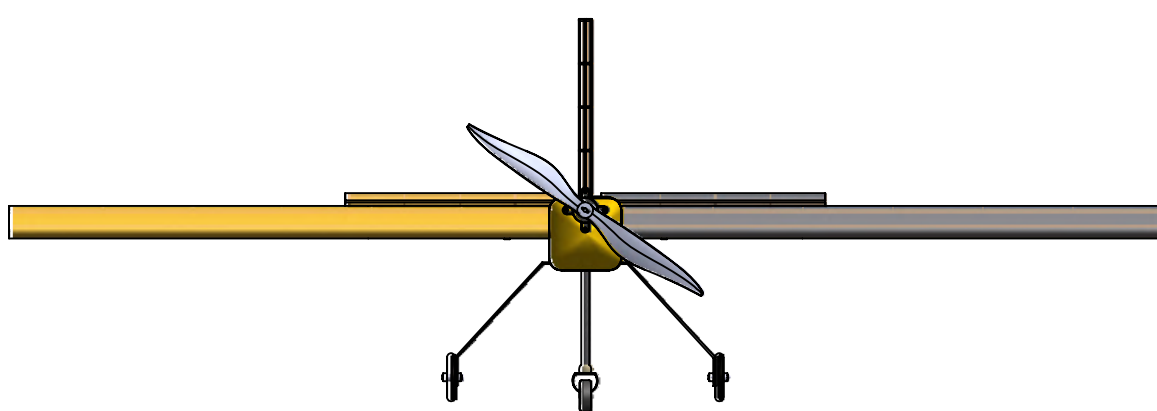
F

Mission 1



E

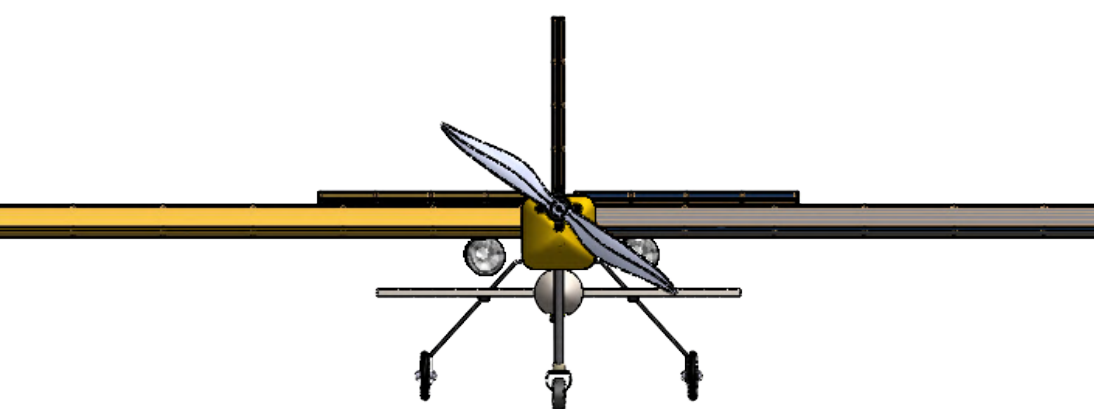
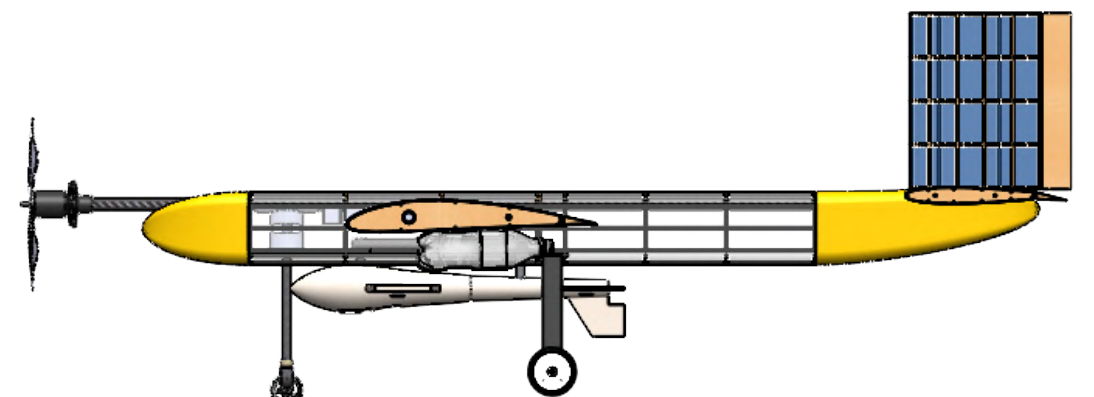
E



D

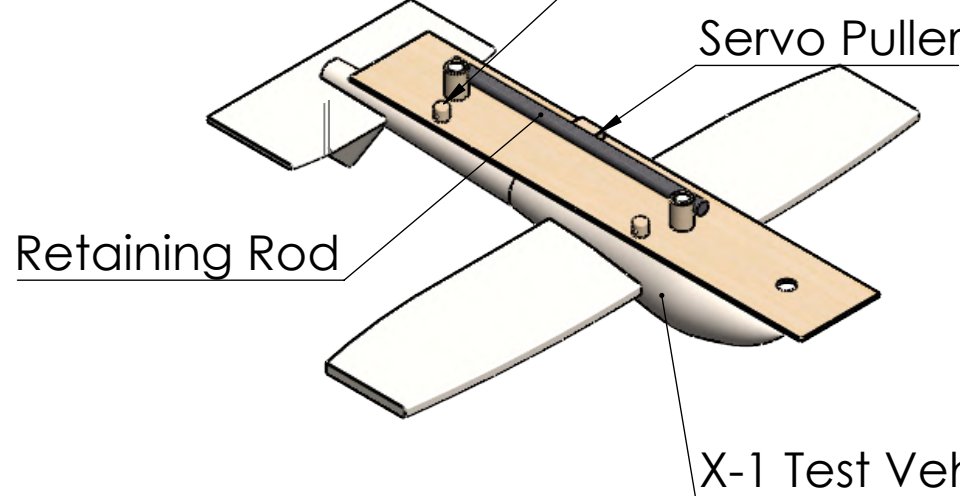
D

Mission 2 & 3



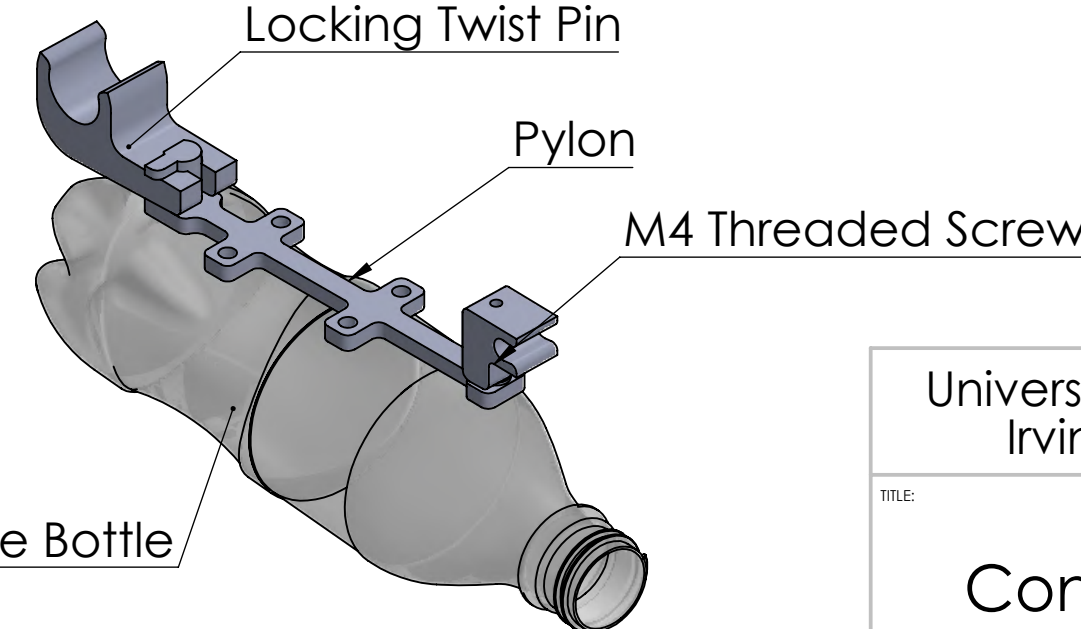
C

C

Elastic Band to Retaining Rod

B

B

Retaining Rod

A

A

University Of California,
Irvine 2024-2025

TITLE:

Mission Configurations

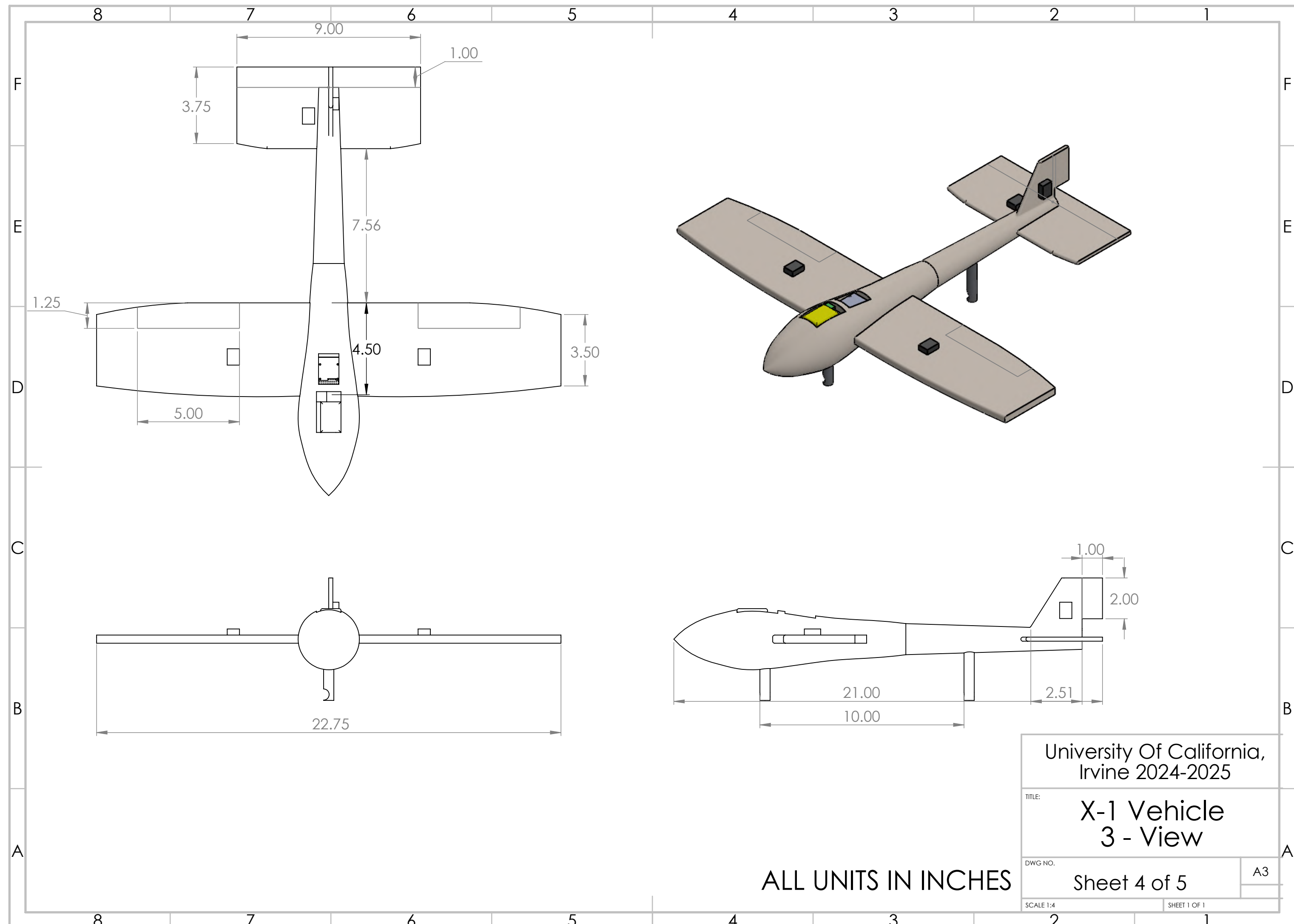
Sheet 3 of 5

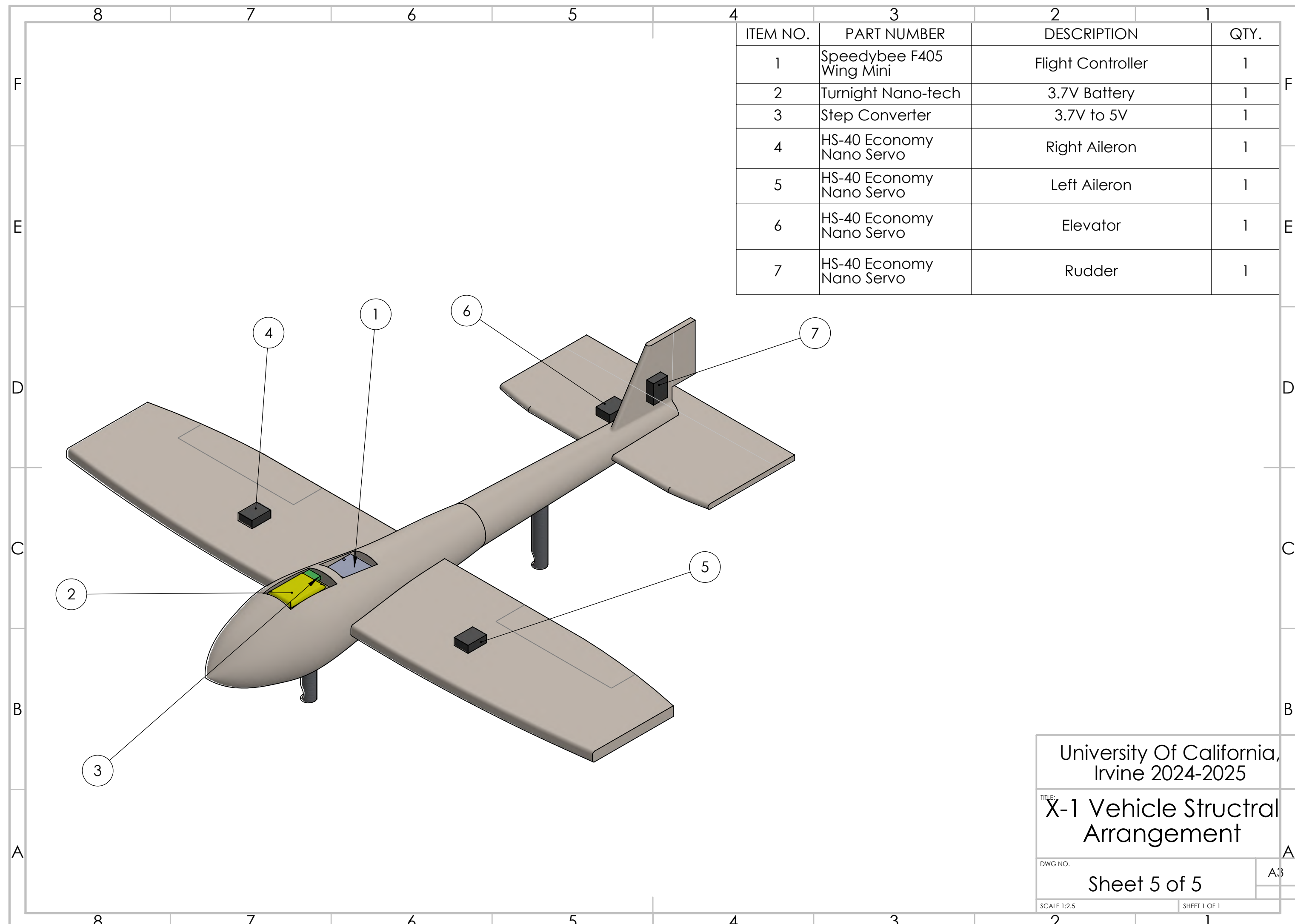
DWG NO.

SCALE 1:12

SHEET 1 OF 1

A3





6. Manufacturing Plan

6.1 Manufacturing Processes

6.1.1 *Balsa Built-Up*

The balsa built-up construction method involves assembling lightweight, durable structures using balsa wood as the primary material. This technique is applied to wings, tails, and the fuselage to create a lightweight yet structurally sound aircraft. The assembly begins by preparing key structural components, including ribs, bulkheads, spars, and stringers. These components are cut from balsa wood to precise dimensions to ensure proper fit and alignment during assembly.

For the wings and tails, a jig system is often used to hold ribs in place at evenly spaced intervals, ensuring accurate alignment throughout the build process. Spars and stringers are inserted into pre-cut slots within the ribs to provide longitudinal support. Cyanoacrylate (CA) glue is used to bond all components because of its fast-curing and strong adhesive properties. Once the ribs, spars, and stringers are securely assembled, balsa sheeting is applied to the structure. This sheeting adds rigidity and helps maintain the intended shape of the wings and tails. The sheeting is carefully positioned to ensure smooth surfaces and proper airfoil contours.

For fuselage construction, bulkheads are positioned along a central support, with stringers running longitudinally to connect the bulkheads. These stringers provide additional structural support and serve as a base for the outer balsa sheeting. The bulkheads and stringers are bonded with CA glue to ensure a strong, lightweight frame. After the framework is assembled, balsa sheeting is used to enclose the fuselage, providing a smooth outer surface and additional strength. Access panels or doors may be incorporated into the sheeting to allow for the placement or removal of internal components. Overall, the balsa built-up method relies on careful cutting, alignment, and bonding of balsa wood components to create lightweight, durable aircraft structures with excellent aerodynamic performance.

6.1.2 *3D-Printing*

3D printing is an additive manufacturing process that builds an object layer by layer from digital designs. This technique creates complex shapes that would be difficult to produce with traditional manufacturing methods. A wide range of materials can be used, including plastics, metals, and composites, making 3D printing suitable for various applications. It is particularly useful for producing small, intricate parts such as spar brackets and connection pieces, where precision and detail are essential.

One of the most common and accessible 3D printing methods is Fused Deposition Modeling (FDM), which uses thermoplastic filaments that are melted and extruded through a nozzle. The strength of printed parts depends on factors such as layer adhesion and printing orientation, as the bond between layers is often weaker than the material itself. Additionally, the infill percentage of a print can be adjusted to enhance strength, though higher infill increases weight and material usage. This flexibility allows users to balance durability, weight, and cost based on specific needs.

6.1.3 *Foam Cutting*

Foam cutting is a precision manufacturing process used to shape polystyrene foam into specific designs, specifically control surfaces for the wing. This process utilizes CNC hot wire cutting, where a heated wire follows programmed paths to slice through the foam with high accuracy. The cutting process is guided by a DAT file containing the airfoil shape,

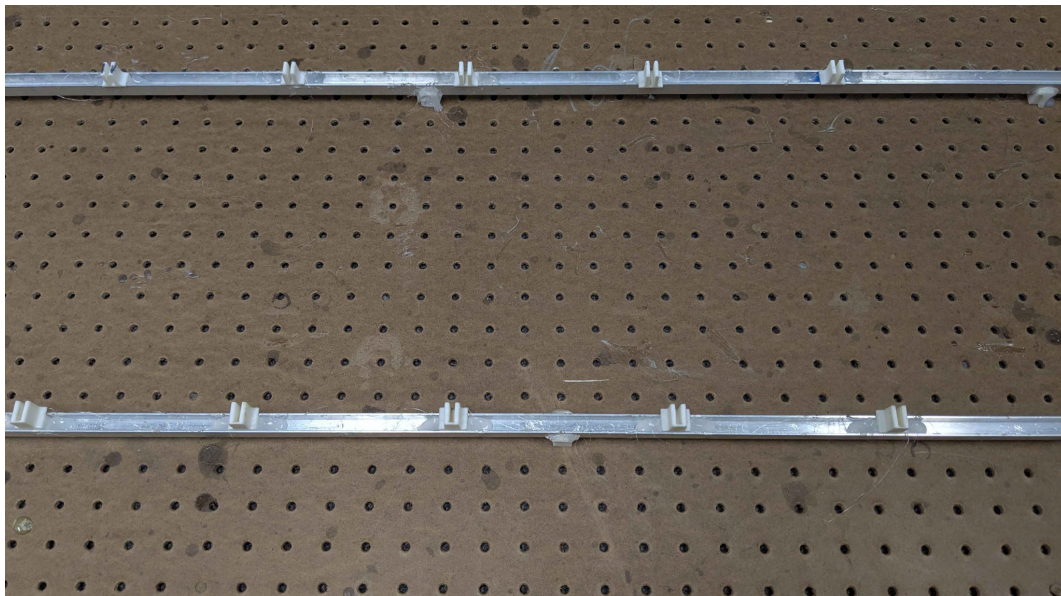
ensuring the final product adheres to the intended aerodynamic design. Since polystyrene foam is lightweight and easy to machine, this method is ideal for producing efficient control surfaces that enhance the flight performance of the aircraft.

6.2 Selected Processes

6.2.1 Wing

A carbon-fiber reinforced built-up balsa structure was selected for the wing due to the balance of structural strength and low weight. The wing structure is made up of 1/8" laser-cut balsa ribs aligned using a jig shown in Figure 32. The jig allows for consistent spacing between ribs and quick adjustments in the event of design changes. After alignment, the ribs are joined by inserting the main and rear carbon fiber rods and hand-cut balsa stringers. The pieces are held together using CA.

Figure 32: Wing Jig



The leading edge of the ribs are inset by 1/32" to allow for a layer of balsa sheeting. This layer helps ensure the leading edge remains smooth and follows the shape of the airfoil. Similarly, the trailing edge of the inboard ribs are supported by foam inserts to help the surface maintain its shape. The wing is covered using monokote to provide a skin. A completed wing is shown in Figure 33.

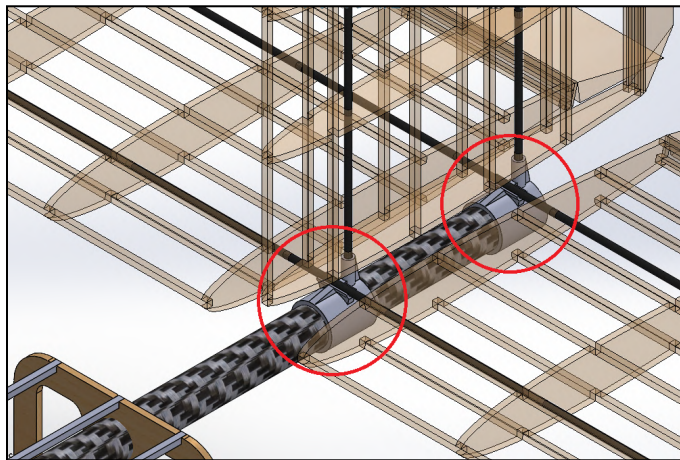
Figure 33: Wing Assembly



6.2.2 Empennage

The tail assembly is constructed using the same method as the wing with 1/16" ribs and a separate jig. The individual tails are connected to the boom using a 3D-printed connection shown in Figure 34. The tails are then attached to the boom using kevlar and epoxy.

Figure 34: Tail Connection



6.2.3 X-1 Test Vehicle

After many attempts to manufacture the X-1 test vehicle out of white foam board, a decision was made to buy off-the-shelf gliders that have been molded and pressed at the factory. Due to limited manufacturing capabilities, creating a glider that flies as well and is as durable would have been a difficult challenge. While researching various gliders online, the Firefox Hand Glider was found to have dimensions closely matching the original sizing intended to accommodate the electronic

package. The bought glider was then cut to add control surfaces as well as a battery, GPS, and Speedybee flight controller in order to turn it into the X-1 test vehicle.

6.2.4 Fuselage

The fuselage is a built-up plywood and balsa structure assembled in a similar fashion to the wings and empennage. Once the bulkheads are aligned, the carbon fiber boom and stringers are inserted and CA is applied to hold them in place. Figure 35 shows the bulkhead at this stage. A plywood floor is laser-cut and attached to the bottom of the bulkheads using CA. The fuselage is then covered with 1/32" sheeting to provide resistance to twisting about the boom and monokote is applied over the sheeting to provide a smooth surface.

Figure 35: Fuselage Jig Setup



6.2.5 Landing Gear

The nose landing gear is constructed using a carbon fiber rod attached to a carbon fiber U-plate by a 3D-printed connection. The 2.5" wheel is connected by a steel axle which connects to nylon bearings housed in the U-plate. The rod is inserted into a 3D-printed mount and an arm is affixed to the top of the carbon fiber rod using CA. The mount and servo box are epoxied to the main boom. The nose gear is shown in Figure 36.

The main gear is an off-the-shelf carbon fiber part with holes drilled into the upper surface for mounting to the fuselage. The 3" wheels are attached using small carbon fiber rods, secured by 3D-printed end caps and epoxied. The main gear is shown in Figure 37.

Figure 36: Nose Gear



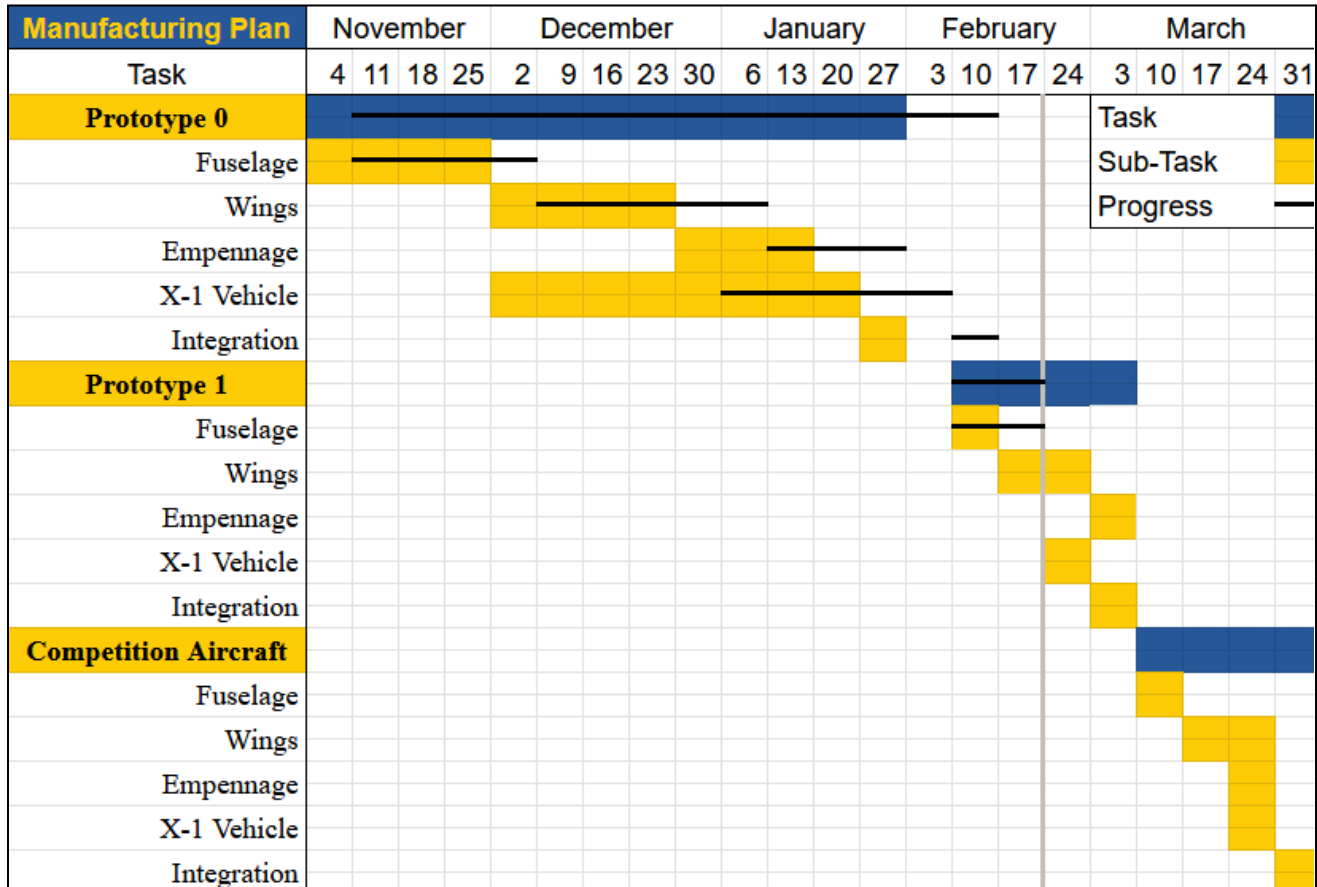
Figure 37: Main Gear



6.3 Manufacturing Milestones

The manufacturing milestones chart, shown in Figure 38, was used to structure the manufacturing timeline by highlighting the major subsystems of each aircraft. The development of Prototype 0 is lengthier to account for the design process and potential changes throughout manufacturing.

Figure 38: Manufacturing Milestones Chart



7. Testing Plan

7.1 Testing Schedule

The schedule and a summary of objectives for ground and flight testing are shown in Table 22.

Table 22: Testing Schedule and Objectives

Planned Date	Actual Date	Test	Objectives
Ground Testing			
11-25-2024	12-14-2024	Wing Deflection	<ul style="list-style-type: none">- Withstand expected loads with a FoS of 1.5- Deflect less than 15% of span- Validate FEA analysis
12-2-2024	1-30-2025	Landing Gear	<ul style="list-style-type: none">- Withstand static loads with a FoS of 1.5- Withstand a dynamic drop test based on maximum sink rate with a FoS of 1.5- Validate FEA analysis
11-2-2024	2-6-2025	Static Thrust	<ul style="list-style-type: none">- Establish a baseline comparison of performance of different propulsion packages
2-17-2025	-	Ground Mission	<ul style="list-style-type: none">- Predict expected score for Ground Mission- Optimize approach to maximize score
Flight Testing			
1-11-2025	-	Prototype 1	<ul style="list-style-type: none">- Demonstrate flight of the aircraft- Simulate M1- Collect flight performance data and compare to predicted performance
3-1-2025	-	Prototype 2	<ul style="list-style-type: none">- Evaluate the effect of changes made- Simulate M2 with 7 lbs of fuel tank weight- Simulate M3 with successful X-1 test vehicle deployment and landing- Collect flight performance data
4-5-2025	-	Competition	<ul style="list-style-type: none">- Demonstrate flight of the aircraft- Collect final flight performance data

7.2 Ground Testing

Ground tests were performed to validate simulations and predict performance calculations. Results from these tests were used to reiterate the design of the *AnteAir* to improve mission scores and guarantee flight readiness.

7.2.1 Checklist

For all tests, basic safety precautions were implemented and verified in the form of a checklist. Table 23 shows a sample checklist used for the ground mission and thrust testing.

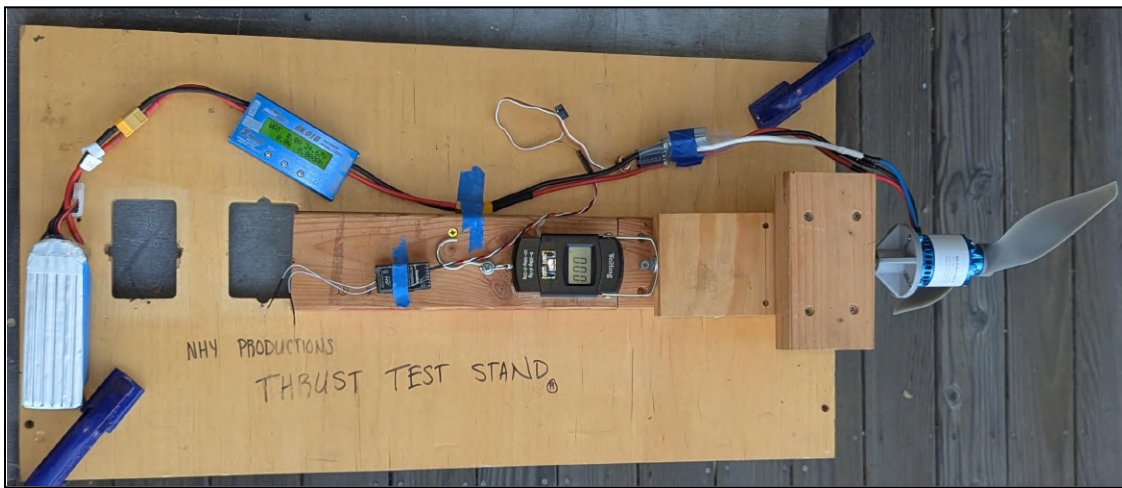
Table 23: Ground Mission and Static Thrust Test Checklist

Ground Mission Test Checklist			Static Thrust Test Checklist		
Landing gear	CHECKED	<input type="checkbox"/>	Motor	SECURED, ROTATES FREELY	<input type="checkbox"/>
Pylons	PREPARED	<input type="checkbox"/>	Propeller	SECURED, NO DAMAGES	<input type="checkbox"/>
Wing Attachment	SECURED, NO DAMAGES	<input type="checkbox"/>	Battery Voltages	VERIFIED	<input type="checkbox"/>
Payload X-1 Test Vehicle	SECURED	<input type="checkbox"/>	Battery	SECURED	<input type="checkbox"/>
Payload fuel tanks	SECURED	<input type="checkbox"/>	ESC setting	CORRECT	<input type="checkbox"/>
Flight controls	CHECKED, WORKING	<input type="checkbox"/>	ESC	CONNECTED	<input type="checkbox"/>
			Wiring	CHECKED	<input type="checkbox"/>
			Measuring Devices	CONNECTED	<input type="checkbox"/>
			Propeller area	CLEAR	<input type="checkbox"/>
			PPE	APPLIED	<input type="checkbox"/>
			Failsafe mode	PREPARED	<input type="checkbox"/>
			Failsafe mode	PREPARED	<input type="checkbox"/>

7.2.2 Static Thrust

Thrust and current draw data for various motor and propeller combinations were gathered through a series of static thrust tests. The testing jig, shown in Figure 39, consisted of a motor and propeller combination, a motor mount that moved along rails attached to a digital fish scale, an ESC, a watt meter, battery, and receiver controlled by a transmitter.

Figure 39: Thrust Testing Rig



7.2.3 Wing Deflection

The structural characteristics of the wing were examined through a deflection test. In this test, the wing was fixed at the root and weight was distributed across the span to simulate the lift forces experienced during flight. Deflection at the root was measured. The wing was tested up to 150% of the expected load during turns, or 4Gs. To be considered structurally sound, the wing was expected to deflect less than 15% of the length of the half span based on FEA analysis and prior experience.

Figure 40: Wing Deflection Test



The effects of the fuel tank load were assessed by applying a force in the opposite direction of the weights equal to 7 lbs, or 150% of the maximum fuel tank weight at the point of attachment. The wing was examined for structural damage.

7.2.4 Landing Gear

Two tests were performed to evaluate the strength and integration of the main and nose gears. In a static load test, the landing gears were attached to a testing platform and loaded to 200% of the fully loaded weight. The test is shown in Figure 41. The landing gears' bending properties were observed, and the gears were inspected for structural damage.

Figure 41: Landing Gear Loading Test



A drop test evaluated the integration of the landing gear into the fuselage. The landing gear and fuselage were dropped from a height of 10 inches to simulate an impact at the maximum sink rate of the aircraft. The aircraft was inspected for structural damage. The setup is shown in Figure 42.

Figure 42: Landing Gear Drop Test



7.2.5 Ground Mission

The GM was simulated to predict scoring for the competition and optimize both the aircraft design and ground mission procedure. Results were used to reassess the importance of the GM with respect to the other missions.

7.3 Flight Testing

Flight testing was performed to validate performance estimates and gather data to characterize and improve *AnteAtAir*. In accordance with the flight schedule and objectives, three separate flights were planned to progressively test the capabilities of the aircraft until competition.

7.3.1 Checklist

Before each flight, the flight readiness of the aircraft was assessed with the aid of a checklist. The checklist ensures safety during all phases of flight and ensures conditions are suitable for testing. An example checklist is shown in Table 24.

Table 24: Flight checklist

Pre-flight			Post-Flight		
Aircraft Exterior	NO DAMAGES	<input type="checkbox"/>	Arming Plug	REMOVED, SAFE	<input type="checkbox"/>
Landing Gear	NO DAMAGES	<input type="checkbox"/>	RX Power	OFF	<input type="checkbox"/>
Aircraft Interior	NO DAMAGES	<input type="checkbox"/>	TX Master Switch	OFF	<input type="checkbox"/>
Battery	INSERTED AND ATTACHED	<input type="checkbox"/>	Battery	REMOVED	<input type="checkbox"/>
CoG	CHECKED WITHIN LIMITS	<input type="checkbox"/>	X-1 Test Vehicle	SECURED	<input type="checkbox"/>
Weather Conditions	FLYABLE	<input type="checkbox"/>	Fuel Tanks	SECURED	<input type="checkbox"/>
Air & Ground Traffic	CLEAR	<input type="checkbox"/>	Mission 2 ONLY		
TX & Power Receiver	ON	<input type="checkbox"/>	X-1 Test Vehicle	SECURED	<input type="checkbox"/>
Control Surfaces	CHECKED, FUNCTIONAL	<input type="checkbox"/>	Fuel Tanks	SECURED	<input type="checkbox"/>
Propeller area	CHECKED, CLEAR	<input type="checkbox"/>	Mission 3 ONLY		
Arming Plug	INSERTED	<input type="checkbox"/>	X-1 Test Vehicle	SECURED, READY TO FLY	<input type="checkbox"/>
Propulsion	WORKING	<input type="checkbox"/>			

8. Performance Results

8.1 Propulsion

Data was collected at 6 different throttle intervals. From the analyzed data, the SunnySky X4130-7 380 KV motor and the 18x10E propeller combination were chosen. Data for this motor in combination with different propellers is visualized below as thrust vs. current and thrust vs. throttle graphs in Figures 43 and 44.

Figure 43: Thrust vs Current

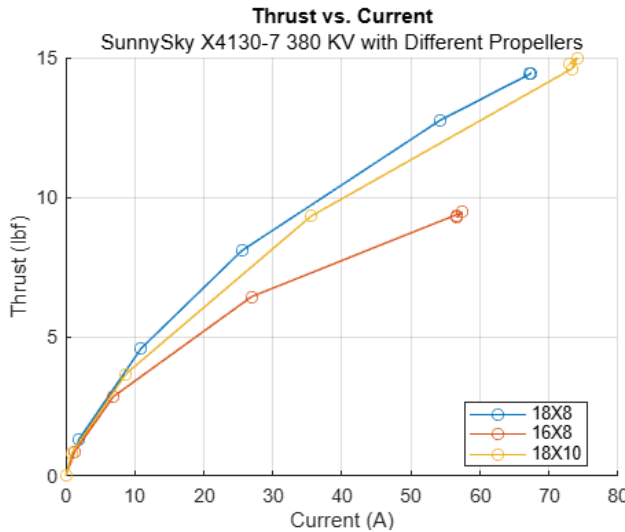
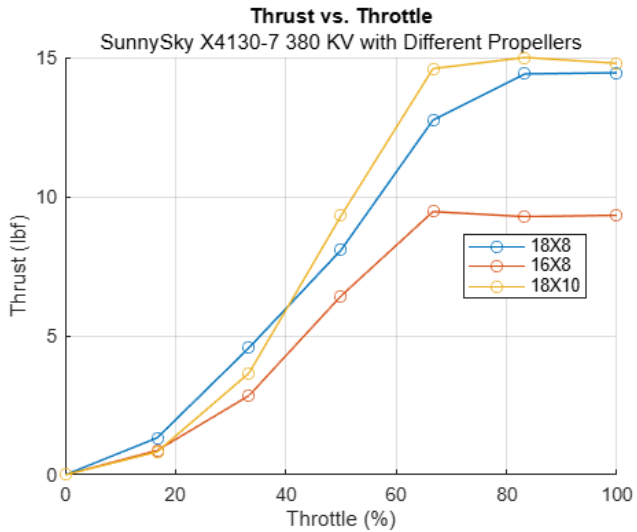


Figure 44: Thrust vs Throttle



Static thrust testing was conducted on the SunnySky X4130-7-380 KV to determine what the best propeller would be to use on the airplane. Shown in Figures 43 and 44, the following propellers were tested using a thrust stand that we created: 18X8, 16X8, and 18X10. The data was collected at 1% throttle intervals to be able to capture performance differences. Based on the data we collected, our motor- the SunnySky X4130-7-380 KV- was the most successful with the 18X10E propeller.

8.2 Structure

The wing deflection test yielded a deflection of 2.20" or 6.11% of the half-span. This was within the acceptable limit of 15%.

The landing gear drop testing of Prototype 0 resulted in structural damage due to shear forces across the bulkhead. To prevent this, the aircraft was redesigned with plywood bulkheads capable of absorbing the impact. After the change, no damage was observed across all of the structural tests.

8.3 X-1 Test Vehicle

8.3.1 Stability Test

To simulate steady level flight with assistance from a flight controller, a stability test was performed. The X-1 test vehicle was set up with moving control surfaces and put into horizon mode, a mode where the X-1 test vehicle would try to stay as horizontal as possible. The vehicle was then tilted to simulate a pitch, yaw, and rolling change.

Through this test, it was observed that the ailerons or elevator would move in an opposite direction as intended. This indicates that the servo direction needed to be in reverse in order to compensate for the instability changes. This was fixed through the INAV system.

8.3.2 Waypoint Test

To simulate the autonomous flight path of the X-1 test vehicle, a comprehensive Waypoint Test was conducted to evaluate the navigation and flight capabilities. Using INAV and referencing the dimensions of the bonus boxes, individual Waypoints were precisely mapped and optimized. Once the waypoints were programmed as depicted in Figure 45 below, the glider was manually guided through each waypoint to ensure that the glider executed a smooth 180-degree turn when necessary and reacted correctly to the individual waypoints.

During the Waypoint Test, the glider did not achieve the expected turn angle. Further investigation revealed that the ailerons and rudder were not responding as intended, affecting maneuverability. Adjustments to the control surface trim were made and it was noted to be more attentive when trimming the control surface as it directly influenced turns. Despite all these changes, the glider proved to be durable and further changes were able to be made until results were satisfactory.

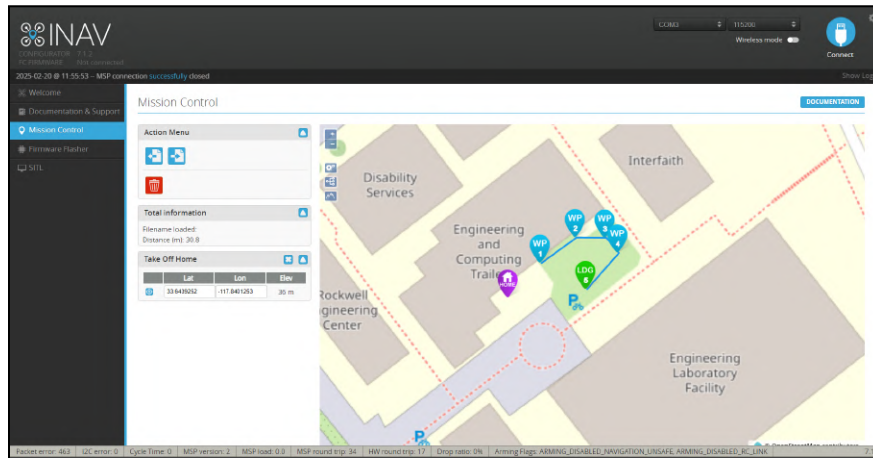


Figure 45: INAV Waypointing

8.3.3 Roof Test

After establishing the waypoints from the Waypoint Test and ensuring the autonomous glider was properly calibrated, the Roof Test was conducted to simulate real-world flight conditions. The glider was launched from the rooftop at the target altitude of 200-400 feet above ground level. Several rounds of testing had to be done with the glider due to the change in elevation affecting the navigation of the waypoints on the glider. After calibrating to a set waypoint of 400 feet, more accurate results were observed.

9. Bibliography

- [1] AIAA, "2024-2025 DBF Rules," Reston, VA, 2024.
- [2] Shevell, Richard S. "Fundamentals of Flight", 2nd ed., Prentice Hall, Englewood Cliffs, N.J, 1989.
- [3] Schaufele, Roger D. "The Elements of Aircraft Preliminary Design", 1st ed, Aries Publication, Santa Ana, CA, 2000
- [4] Raymer, D. P., "Aircraft Design: A Conceptual Approach", 7th ed., AIAA Education Series, American Institute of Aeronautics and Astronautics, Reston, VA, 2023.
- [5] MIL-F-8785C, Flying Qualities of Piloted Planes, Military Specification, 1980
- [6] eCalc, eCalc Aircraft Design Tools, <https://www.ecalc.ch/index.htm/>
- [7] XFLR5, <http://www.xflr5.tech/xflr5.htm/>.
- [8] J. Anderson, Jr, "Aircraft Performance and Design," McGraw, 1999.
- [9] Gowda, S Anagha, "Comparison of Aerodynamic Performance of NACA 4412 and 2412 using Computational Approach," RV College of Engineering, 2019.
- [10] NAU SAE, "Charts and Graphs," NAU SAE Aero
- [11] MIL-F-8785C, Flying Qualities of Piloted Planes, Military Specification, 1980
- [12] Munson, Bruce R. "Fundamentals of Fluid Mechanics", 9th ed, Wiley, New York, NY:, 2006.
- [13] Markus Müller, eCalc, 2025
- [14] "SOLIDWORKS 2023-24", Dassault Systemès SOLIDWORKS Corp. Available: <https://www.solidworks.com/>. [Accessed 2024]
- [15] MATLAB: programming and numeric computing platform, <https://www.mathworks.com/products/matlab.html>
- [16] PythonCoreTeam, Python: A dynamic open source programming, Python Software Foundation [online], <https://www.python.org>.